

Design of microstructure in electrochemical devices by
electrophoretic deposition for their performance improvement

電気泳動堆積法による電気化学素子の微構造設計と特性向上

February 2017

DOCTOR OF ENGINEERING

SHOTA AZUMA

TOYOHASHI UNIVERSITY OF TECHNOLOGY

Contents

Chapter I. General introduction	1
Chapter II. Development of multilayer coating system based on electrophoretic deposition process	
2.1. Introduction	7
2.2. Experimental	8
2.2.1. Concept of the EPD system	8
2.2.1.1. System configuration and Detail of units	9
2.2.1.1.1. Control unit	9
2.2.1.1.2. Power supply unit	9
2.2.1.1.3. Transfer arm with electrode	9
2.2.1.1.4. Rotatable beakers holder	10
2.2.1.1.5. Washing unit	10
2.2.1.1.6. Dryer	10
2.2.1.1.7. Data analyzer	10
2.2.2. Multilayers preparation procedure	10
2.2.2.1. Preparation of suspensions	10
2.2.2.2. Alternately deposited multilayered films	11
2.3. Results and discussion	11
2.4. Conclusion	13
References of chapter 2	13
Figures of chapter 2	15
Chapter III. Investigation electrochemical performance and interfacial properties of photoelectrode based on NiTi-layered double hydroxide / reduced graphene oxide composite fabricated by electrophoretic deposition	
3.1. Introduction	25
3.2. Experimental	27
3.2.1. Synthesis of NiTi-layered double hydroxide / reduced graphene oxide composite powder and its dispersion	27

3.2.2. Fabrication of NiTi-layered double hydroxide film coated electrode by electrophoretic deposition	28
3.2.3. Characterization and evaluation of NiTi-layered double hydroxide film-coated electrodes	28
3.3. Results and discussion	29
3.3.1. Characterization of NiTi-layered double hydroxide / reduced graphene oxide composite powder and the composite film-coated electrodes	29
3.3.2. Evaluation of electrochemical performance and interfacial properties of NiTi-layered double hydroxide / reduced graphene oxide in photoelectrochemical systems	30
3.4. Conclusion	33
References of chapter 3	34
Figures of chapter 3	35
Chapter IV. Colloidal processing of $\text{Li}_2\text{S-P}_2\text{S}_5$ films fabricated via electrophoretic deposition and its characterization as solid electrolyte for all solid state lithium ion batteries	
4.1. Introduction	47
4.2. Experimental	49
4.2.1. Preparation of suspension of Li_3PS_4 precursor	49
4.2.2. Deposition of Li_3PS_4 films from Li_3PS_4 precursor film via electrophoretic deposition	49
4.2.3. Characterization of electrophoretic deposition films	50
4.3. Results and discussion	50
4.3.1. Evaluating of dispersion state of Li_3PS_4 precursor in nonpolar-solvent for applied to electrophoretic deposition	50
4.3.2. Characterization of deposited film	51
4.3.3. Evaluation of conduction properties associated with Li_3PS_4 morphology	53
4.4. Conclusion	55
References of chapter 4	56
Figures of chapter 4	57

Chapter V. Preparation of cathodic mixture layers by alternant electrophoretic deposition process and evaluation of charge-discharge cycle performance for all solid state lithium ion batteries	
5.1. Introduction	71
5.2. Experimental	73
5.2.1. Preparation dispersion of $\text{LiNi}_{1/3}\text{Mn}_{1/3}\text{CoO}_2$ and Li_3PS_4 precursor with nonpolar-solvents	73
5.2.2. Fabrication of alternatively stacked $\text{LiNi}_{1/3}\text{Mn}_{1/3}\text{CoO}_2$ and Li_3PS_4 layer by electrophoretic deposition	74
5.2.3. Characterization of alternative stacking layer	74
5.3. Results and discussion	75
5.3.1. Investigation of electrophoretic deposition behavior in $\text{LiNi}_{1/3}\text{Mn}_{1/3}\text{CoO}_2$ and Li_3PS_4 precursor dispersion	75
5.3.2. Deposition of alternatively stacked $\text{LiNi}_{1/3}\text{Mn}_{1/3}\text{CoO}_2$ and Li_3PS_4 layer	75
5.3.3. Charge-discharge cycle performance of cathodic mixture layer fabricated alternative electrophoretic deposition process	76
5.4. Conclusion	77
References of chapter 5	77
Figures of chapter 5	78
Chapter VI. General conclusion	90
Acknowledgement	92
List of publications	93

Chapter I

General introduction

Power sources as batteries and dynamo are crucial product in the current society which is based on a lot of equipment driven by electricity. Especially, electricity storage systems are strongly required technology for not only popularization of portable devices but also energy crisis. Electrochemical devices, which can convert electric energy and chemical bilaterally, have attracted much interest as promising power source for the next generation such as fuel cells, dye-sensitized solar cells, secondary batteries such as lithium ion batteries and metal-air batteries.

In these devices, functional materials are employed in according to each working principle. Hence, for improving performance of these devices, development of highly functional materials compared with conventional ones is vital. Similarly, optimum fabrication methods involving several types of functional materials with high-performance outcome are required to achieve improved functionality of device. This consideration is essential for the development of novel functional materials.

Coating techniques are the key in the fabrication of a number of functional materials. Unique and novel functionality with desired properties could be obtained from the coatings. Additionally, multi functionality is also achievable by with the formation of multilayered films. Gas-phase methods such as physical vapor deposition (PVD) and chemical vapor deposition (CVD) are employed as typical coating methods due to feasibility to obtain films with high quality and controllable film thickness in order of several 1 ~ 100 nm. However, the setbacks of gas-phase method are as follow:

- (1) Small coating surface area which is not suitable for large scale production
- (2) Difficulty in obtaining thick film with more than 1micrometer thickness
- (3) High-cost consumption.

These problems are mostly attributed to the usage of vacuum environment. On the other hand,

liquid-phase methods (such as sol-gel, electrodeposition, Langmuir-Blodgett, and liquid-phase epitaxy) are relatively low cost with the ability to produce good and consistent quality of films over a large area. However, in term of electrochemical device fabrication, liquid-phase methods face similar problems to that of gas-phase methods, which are the difficulty in obtaining thick film and uncontrollable treatment for microstructure in casted films.

Electrophoretic deposition (EPD) is a unique coating technology categorized under colloidal process; under the influence of electric field, the charged colloids or particles suspension in a fluid are directed and deposited as thick films on the opposed charged electrodes. In contrast to the conventional coating methods mentioned above, EPD technique has the advantages of rapid formation rate, large-area deposition of films with high packing density and controllable thickness at a low-cost. The phenomenon of EPD has been known since 1808 when a Russian scientist known as Ruess observed the electric-field-induced movement of clay particles in water. The first practical use of this technique occurred in 1933 when the deposition of thoria particles on a platinum cathode as an emitter for electron tube application was patented in the USA. Electrophoretic coating began to take its current shape in the late 1950s when Dr. George E. F. Brewer and the Ford Motor Company team began working on developing the process for the coating of automobiles. The first commercial anodic automotive system began operation in 1963. This process is industrially used for applying coatings to metal fabricated products. It has been widely used to coat automobile components, tractors, heavy equipment, electrical switch gear, appliances, metal furniture, beverage containers, fasteners, and many other industrial products (too many examples). Although the basic phenomena involved in EPD are well known and have been the subject of extensive theoretical and experimental research, the EPD of ceramics was first studied by Hamaker, and only in the 1980s did the process receive attention in the field of advanced ceramics. There is general agreement in the scientific community that further R&D work needs to be done to develop a full quantitative understanding of

the fundamental mechanisms of EPD to optimize the working parameters for a broader use of EPD in materials processing.

Compared to other advanced shaping techniques, the EPD process is very versatile since it can be modified easily for a specific application. Numerous applications of EPD have been developed for the fabrication of ceramics, including the preparation of coatings, fiber-reinforced composites, laminated materials, porous membranes, stepwise functionally graded materials and continuously graded materials. In this way, various materials structure in microscale can be extensively designed by using EPD technique with optimized conditions for each structures fabrication. In addition, the EPD is also gaining increasing interest as a coating technique for novel films with intrinsic heterostructure of nano/micro particle scale. Optimized heterostructures are promising in achieving combined functionalities in a single material. However, in conventional methods such as gas-phase and liquid-phase methods, films with homogeneous structure are obtained due to deposition of chemicals which are dispersed as ion and molecule in gas or liquid forms. Hence, according to their principles, introducing hierarchical heterostructure including nano/micro particle size scale into the films is difficult. For instance, fabrication of films based on composited particles prepared as core-shell type cannot be obtained using these conventional methods in general. Therefore, the functionality is limited due to the difficulty of materials design. On the other hand, by employing EPD, films with hierarchical heterostructure in the scale of nano/micro could be obtained due to the utilization of as-prepared composite particles suspensions. Various types of composite particles are applied when surface charges, for electrical dispersing in suspending media, are generated on particles surface.

Moreover, motion of electrophoretic particles, which will generate the films, in EPD process can be controlled by adjusting the applied electric field. Thus, by controlling the deposition patterns, the design of film with higher order is achievable. Interestingly, wide range hierarchical films which are

unable to be obtained by conventional method could be prepared by carefully combining choice of suspensions and adjustment of electric field conditions. Therefore, the EPD technique has great potentials in improving the performance of materials with multi-functionalities, which are applicable for electrochemical devices.

In this works, EPD was employed for fabrication of electrochemical devices such as photoelectrochemical cells and all-solid-state lithium ion batteries, with performance evaluations being carried out. This doctoral thesis consists of 6 contents including 4 chapters indicated below:

Chapter 1 General introduction

It shows the background and the objectives in this study.

Chapter II

The automatic multilayer coating system used in this work, based on electrophoretic deposition process, which includes coating, drying, and washing, is proposed for stable and effective preparation of multilayered films. Multilayered structures are one of the target structures in the fabrication of functional materials by EPD because they are favorable for significantly enhancing the properties of electrochemical devices and for device integration. As demonstration of the system, multilayered films consisting of layers of $\text{LiNi}_{1/3}\text{Mn}_{1/3}\text{Co}_{1/3}\text{O}_2$ (NMC) and Al_2O_3 particles were fabricated under constant applied voltage and current. Results indicate that film structures, such as the thicknesses of the inner layers and number of layers are controllable by varying conditions of processes flow in a simple operation. The EPD system is also expected to be applied for the preparation of particle-reinforced composite materials, which has been attempted in this work too.

Chapter III

In this chapter, as study case of performance evaluation of functional film, with controlled nanostructure, the composite films of NiTi-layered double hydroxide (NiTi-LDH, $[\text{Ni}_{1-x}\text{Ti}_x(\text{OH})_2]^{2x+}(\text{A}^{n-})_{2x/n} \cdot m\text{H}_2\text{O}$) with various contents of reduced graphene oxide (rGO) were prepared by the EPD; these composites were employed as a visible-light responsive photoanode in photoelectrochemical cells based on Honda-Fujishima effect. The approximately 10 μm -thick NiTi-LDH/rGO films were deposited on fluorine-doped tin oxide (FTO) glass. The rGO containing films of NiTi-LDH/rGO|FTO showed a higher photovoltage than the film without rGO of NiTi-LDH|FTO. Electrokinetic parameters, especially photogeneration rate and chemical capacitance, were significantly affected by increasing Ti^{3+} surface defects due to the hybridization with rGO. The increase in these two parameters predominately contributed to the enhancement of the photovoltage. The expected effects due to the nanocomposite structure were also observed substantially in the performance of the composites-based EPD films employed as photoanode, which showed highly sensitive in both their structure nanoscale structure and microscale structure.

Chapter IV

In this chapter, EPD technique was also employed in the preparation of effective solid-state electrolyte layer, based on $\text{Li}_2\text{S-P}_2\text{S}_5$ (LPS) which is a promising key functional material in all-solid-state lithium ion batteries. A suspension of LPS precursor, prepared by liquid shaking (LS) method, was employed in this EPD processing, as novel colloidal coating technique. LS method has been reported in our previous study as a novel method of synthesis of LPS. LPS is not stable in polar solvents, which are the common solvents used in EPD. However, an LPS precursor deposited film was obtained successfully from its precursor suspension in a non-polar solvent because of its

positive surface charge. The homogeneous film thicknesses of 10~100 μm were controllably prepared. An EPD deposited precursor film of LPS, aged by warm pressing, exhibited high conductivity ($1.98 \times 10^{-4} \text{ S cm}^{-1}$), at ambient temperature, and significantly low activation energy (16.6 kJ mol^{-1}), compared with conventional LPS materials. Thus, good solid-solid interfacial contact can be obtained in the sulfide-based ionic conductor by employing EPD process followed by warm pressing.

Chapter V

In this chapter, for application as a cathode in all-solid-state lithium ion batteries, films with ordered multilayer structure of NMC and LPS were fabricated by alternate EPD process using the automatic EPD system, LS method, and novel dispersant for NMC. The specific structure, thickness, and number of layers were controllable by adjusting various conditions in the EPD process. Employing the multilayer film as cathode, the single battery cell exhibited typical charge/discharge behaviors with cell capacity of approximately 25 mAh g^{-1} . In order to achieve a practically applicable cathode, the films structures should be optimized by adjusting for optimal conditions in the EPD process.

Chapter VI General conclusion

The conclusions of this thesis are described in this content.

Chapter II

Development of multilayer coating system based on electrophoretic deposition process

2.1. Introduction

Ceramic materials have been increasingly used in a broad range of industries including biotechnology, pharmaceutical, dairy, food, and beverage, the chemical and petrochemical, microelectronics, metal finishing, and power sources. In the latter, ceramics have been employed in solid oxide fuel cells¹⁾, solid oxide electrolysis cells²⁾, secondary batteries such as lithium ion batteries³⁾, thermo-electronic devices⁴⁾ and solar cells⁵⁾. Recently, films with realizable complex structures are highly desired to have diverse multifunctions. For instance, homogeneous or multi-stratified films with controllable density of deposited particles, porosity and composite with different materials are all promising studies.

The fabrication of multilayered ceramics is a significant technique in the producing energy devices like capacitors⁶⁾, thermo-electric devices⁷⁾ and tandem type dye-sensitized solar cells⁸⁾. The development and commercialization of multilayer ceramic capacitors have been significant factors leading to size reduction of a variety of electrical circuits due to the micron-scale spacing of interleaved electrodes and high dielectric ceramics in multilayer ceramic capacitors provides exceptionally high capacitance in small volumes⁶⁾. Multilayered ceramics are often obtained by tape casting⁹⁻¹¹⁾ and screen printing¹¹⁻¹²⁾ due to their simplicity and quickness. However, conventional methods have drawbacks as follows:

- (1) Inability to obtain large area device with uniform quality.
- (2) Difficult to obtain thicker film and thickness control.
- (3) Coated substrates are limited to planar surface.
- (4) Microstructure in casted films is uncontrollable.

Electrophoretic deposition (EPD) is an important technique for colloidal coating¹³⁻¹⁴⁾, which has the advantages of rapid, large-area deposition of films with high packing density and controllable thickness at a low-cost. It uses applied electric fields, to move electrically charged colloids or particles in suspension towards electrodes and finally to form films deposition; the electrode shape is flexible depending on the practical applications. Normally, the preparation of multilayered films by EPD is just at laboratory scale; complicated procedures including inserting/removing electrode substrates into/from EPD bath suspensions, electric field applying, drying, and washing, are manually controlled. Therefore, the multilayered films (consisted with relatively thinner layers, ex. 1~10 μm) obtained from manual process are nearly unrepeatable because of wide range of the procedures.

Therefore, the automatic multilayer coating system based on electrophoretic deposition process is proposed in this study. By introducing this system, rapid progress is expected in the functional films preparation with highly ordered architecture.

2.2. Experimental

2.2.1 Concept of the EPD system

Fig. 2-1 shows the photograph of the main unit of the automatic EPD system, and the block diagram of the EPD system is depicted in Fig. 2-2. In the automatic mode, three following functions can be programmed in any sequences (Fig. 2-3).

- (1) Coating: in this function, EPD process can be operated under variable conditions. For instance, the deposition time, working mode (at constant voltage or constant current) and the wave shape can be all controlled.
- (2) Drying: during this process, the hanging specimens are blown with heated air. Tunable airflow and heater are applied to control the flow rate and temperature.

(3) Washing: Specimens can repeatedly be dipped into solvent and then withdrawn until they are well cleaned. Any solvent can be injected in and drained out automatically by a digital controlled pump.

The program allows no more than 14 processes in one working period. It can be repeated for at most 999 times.

2.2.1.1 System configuration and Detail of units

This includes a touch-panel used as the control center, the EPD system is assembled by the following units:

2.2.1.1.1. Control unit

With power supply unit and a programmable logic controller inside, control unit coordinate every part to work according to the scheduled program.

2.2.1.1.2 Power supply unit

DC power supply (Yokogawa Electric Co.) is used to apply not only constant voltage/current but also any editable wave shape during EPD process. The operation time is controlled by the touch-panel.

Specifications of the power supply are shown as follows:

(1) Output:

- Voltage: 0 ~ ± 110 V
- Current: 0 ~ ± 3.2 A

(2) Resolution: 100 μ sec

(4) Instantaneous voltage/current information can be saved for further analysis during application.

2.2.1.1.3 Transfer arm with electrode

Holding the specimens, the transfer arm can move it to 3 locations for different processes. It also has a function to immerse the specimens into the beakers during the EPD and washing process. All the movements are digitally controlled by the touch-panel.

Additionally, an electrode which can connect the substrate to the DC power supply is also assembled on the transfer arm.

2.2.1.1.4 Rotatable beakers holder

Depending on the processes, by self-rotation, the holder can place the specific beaker underneath the electrode transfer arm. In the rotator, there are three locations for holding different kinds of suspensions. Below each beaker, a speed adjustable stirrer is set to give continuous/discontinue mixing for the whole EPD process.

2.2.1.1.5 Washing unit

With this unit, after EPD process, specimens are repeatedly dipped into washing solvents to remove extra particles which are loosely attached on the substrates. Based on specific cases, the dipping times and the frequency can also be adjusted by touch-panel.

2.2.1.1.6 Dryer

Washed specimens are dried by the dryer. The temperature, air flow and heating time are controlled by touch-panel.

2.2.1.1.7 Data analyzer

In order to receive and analyze the voltage/current data during EPD process, a PC was connected to the power supply unit.

2.2.2. Multilayers preparation procedure

2.2.2.1. Preparation of suspensions

The surface of $\text{LiNi}_{1/3}\text{Mn}_{1/3}\text{Co}_{1/3}\text{O}_2$ (NMC, $1\mu\text{m}$) and Al_2O_3 (100 nm) particles were coated with poly(diallyldimethylammonium chloride) (PDDA, M_w :400,000 ~ 500,000, Sigma-Aldrich[®]) by mixing PDDA aqueous solution (10wt.%) followed by ultra-sonication for 30 mins. The modified particles were

dispersed into 2-propanol by ultra-sonication for another 30 min. As a result, the as obtained suspensions of NMC and Al₂O₃ with 3wt.% concentration were then used for the following coating procedures.

2.2.2.2. Alternately deposited multilayered films

EPD was carried out by using indium tin oxide (ITO) coated glass substrate (20×30×0.7 mm) as the anode while on the parallel cathode, similar ITO coated glass was used at a distance of 0.5cm. During EPD process either constant voltage of 50 V or constant current density of 10 μA cm⁻² was applied for 60 s. In order to obtain the multilayered films, the following cycle was repeated for 5 times:

- (1) Coating of Al₂O₃
- (2) Washing
- (3) Drying
- (4) Coating of NMC
- (5) Washing
- (6) Drying

2.3. Results and discussion

The multilayered films obtained consist of alternating EPD by applying 50 V are shown in Fig. 2-4, in which no crack and defect could be observed, owing to the factor well-controlled processes, as it is difficult to obtain this quality manually. Fig. 2-5 and Fig. 2-6 illustrate cross-sectional images of the films with (Al₂O₃|NMC)₅ on ITO glass deposited by applying constant voltage and current density respectively. As shown in these images, multilayered structure formed by NMC (black layers) and Al₂O₃ (white layers) can be clearly observed. The total thicknesses of the multilayers are 250 μm and 46 μm for Fig. 2-5 and Fig. 2-6, respectively. The thicknesses of each layer in the films were controlled by adjusting EPD conditions such as applied voltage, current density, and time. By repeating each coating process, more layers in the films can be achieved. The correlations of each layer thickness and layer number obtained

from Fig. 2-5 and Fig. 2-6 are shown in Fig. 2-7. Even when EPD voltage was kept the same, each film became thinner gradually: thickness of NMC layers and Al_2O_3 layers decreased from 70 μm to 30 μm and from 30 μm to 5 μm , respectively. The thicker the total films are, the thinner the new coated layer became due to the lower deposition rate. In contrast with the constant voltage mode, employing constant current density mode, more consistent layer thickness was apparently formed, which have average thicknesses of 3.2 μm and 6.5 μm for NMC and Al_2O_3 , respectively. Films with homogeneous multilayered structure are crucial in their application. Therefore, it was considered that constant current mode was more suitable for the preparation of uniform multilayered films.

The reason of reduced films thicknesses under applied constant voltage mode is probably due to the resistance increment during films formation. As for constant voltage EPD deposition, increasing resistance in each deposition layer against EPD time and numbers of layers are confirmed in both Al_2O_3 and NMC (Fig. 2-8 (a) and (b)), In other words, newly deposited films on top of the under-layers become thinner under constant applied voltage due to the increased resistivity of the under-layers. Additionally, transition trends of resistance are influenced by various factors such as surface/internal structure of under-layer, particle size, etc. Hence, the precise thickness control of each layer is difficult in the constant voltage mode.

Then, Figs. 9 (a) and (b) explain the voltage transition for EPD of Al_2O_3 and NMC respectively under applying constant current. In corresponding with increased resistance as indicated in Fig. 2-8, the voltage curves exhibit rising trend against EPD time and number of deposited layers. Thus, although higher resistance with increasing number of deposited layers, a thickness of newly formed films on top of under-layer was maintained due to compensated voltage in employing constant current density mode.

Briefly, using this automatic EPD system, over 100 layers can be coated easily if deposition conditions are optimized. Theoretically, according to the specification of the system, at most 999 layers can be formed by simply repeating the program. Furthermore, it is also expected to produce

particle-reinforced composite materials. Schematics of EPD procedure for fabricating this kind of material are illustrated in Fig. 2-10. For example, in the case to prepare a composite film containing two kinds of particles described as A and B, in suspension, A particles are first deposited on the electrode to form a sub-monolayer. Then, followed by replacing the specimen from A suspension into B suspension, B particles are deposited onto so-coated films. Particularly, they would fill the space between A particles. By repeating the processes above, particle-reinforced composite films could be obtained using the automated EPD system. The composite films would be served as electrode in energy devices. In our future study, the automatic EPD system will be employed for the preparation of composited cathode layer in solid-state lithium ion batteries based on sulfide electrolyte.

2.4. Conclusion

In this study, the automated EPD system that includes coating, drying, and washing processes, effective fabrication of multilayered films, which are one of the target structures in the EPD, was demonstrated. As a result, smooth multilayered films without any defects were prepared using this system. The specific microstructures such as the thickness of each layer and their total number were controllable by adjusting detail conditions. The performance of the system has been proven to be qualified for multilayered films preparation. Moreover, we proposed utilizing this system to fabricate particle-reinforced composite films.

References

- 1) N.Q. Minh, *J. Am. Ceram. Soc.*, **76**, 563-588 (1993).
- 2) M. Ni, M.K.H. Leung and D.Y.C. Leung. *Int. J. Hydrog. Energy*, **33**, 2337-2354 (2008).
- 3) J.W. Fergus, *J. Power Sources*, **195**, 4554-4569 (2010).
- 4) S.B. Riffat and X. Ma., *App. Therm. Eng.*, **23**, 913-935 (2003).
- 5) R. Jose, V. Thavasi and S. Ramakrishna, *J. Am. Ceram. Soc.*, **92**, 289-301 (2009).

- 6) H Kishi, Y Mizuno and H Chazono, *Jpn. J. Appl. Phys.*, **42**, 1-5 (2003).
- 7) G.D. Mahan and L. M. Woods, *Phys. Rev. Lett.*, **80**, 4016-4019 (1998).
- 8) A. Mishra, M.K.R. Fischer and P. Bäuerle, *Angew. Chem. Int. Edit.*, **48**, 2474-2499 (2009).
- 9) C. Pithan, D. Hennings and R. Waser, *Int. J. Appl. Ceram. Tec.*, **2**, 1-14 (2005).
- 10) H. Liu and S.M. Hsu. *J J. Am. Ceram. Soc.*, **79**, 2452-2457 (1996).
- 11) D.I. Woodward, I.M. Reaney, G.Y. Yang, E.C. Dickey and C. A. Randall, *Appl. Phys. Lett.*, **84**, 4650-4652 (2004).
- 12) C. Pithan, D. Hennings and R. Waser, *Int. J. App. Ceram. Tec.*, **2**, 1-14 (2005).
- 13) L. Besra and M. Liu, *Prog. Mater. Sci.*, **52**, 1-61 (2007).
- 14) T. Uchikochi, *Micromeritics*, **57**, 36-42 (2014).



Fig. 2-1. Photograph of main unit of the EPD system.

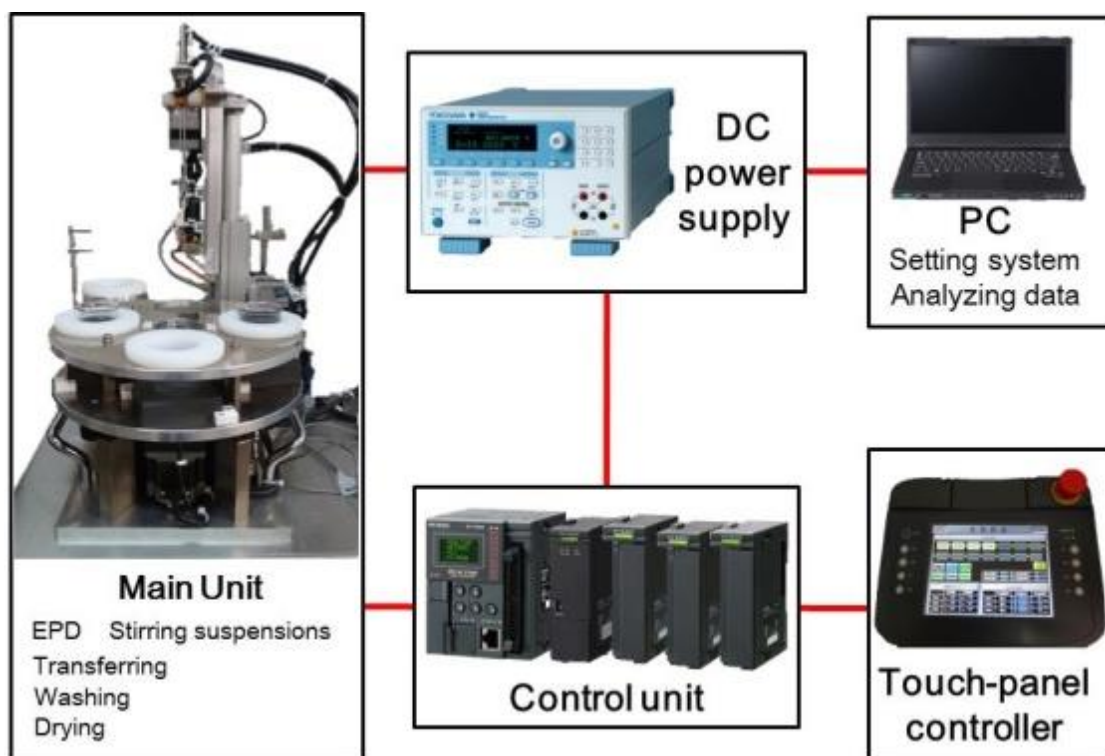


Fig. 2-2. Block diagram of overall EPD system.

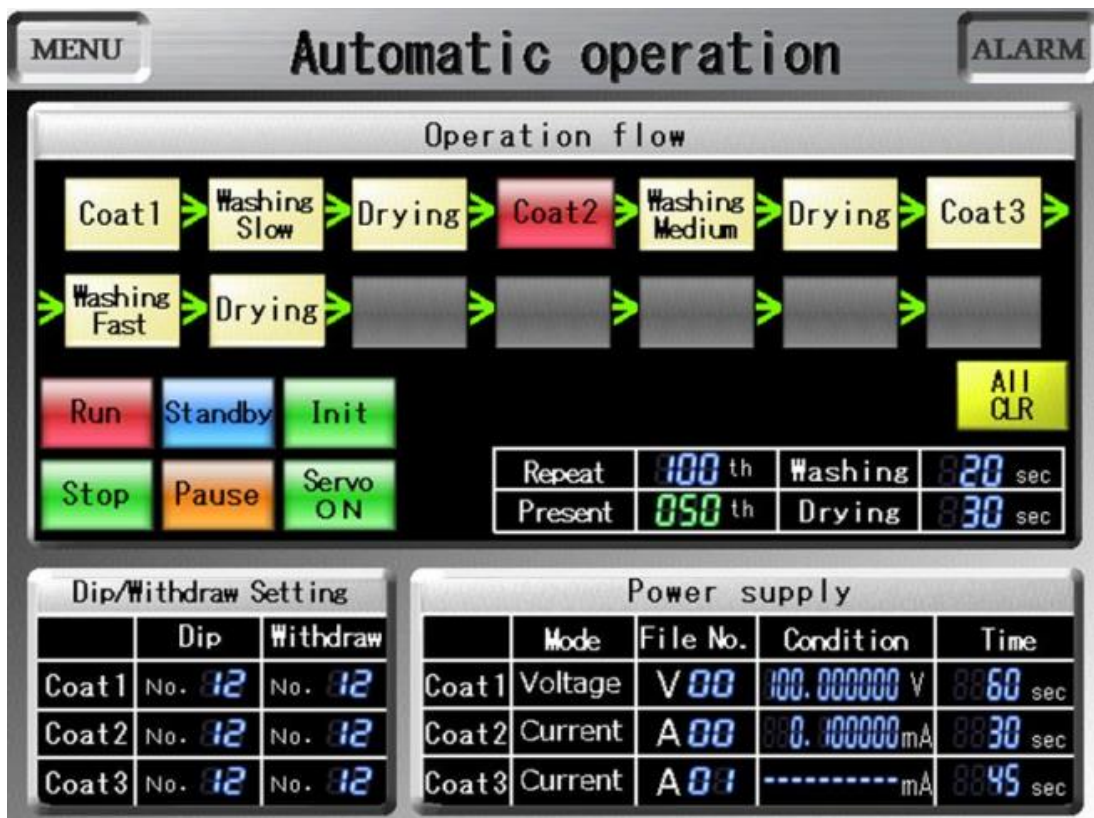


Fig. 2-3. Screen image of automatic operation mode in the touch-panel controller.

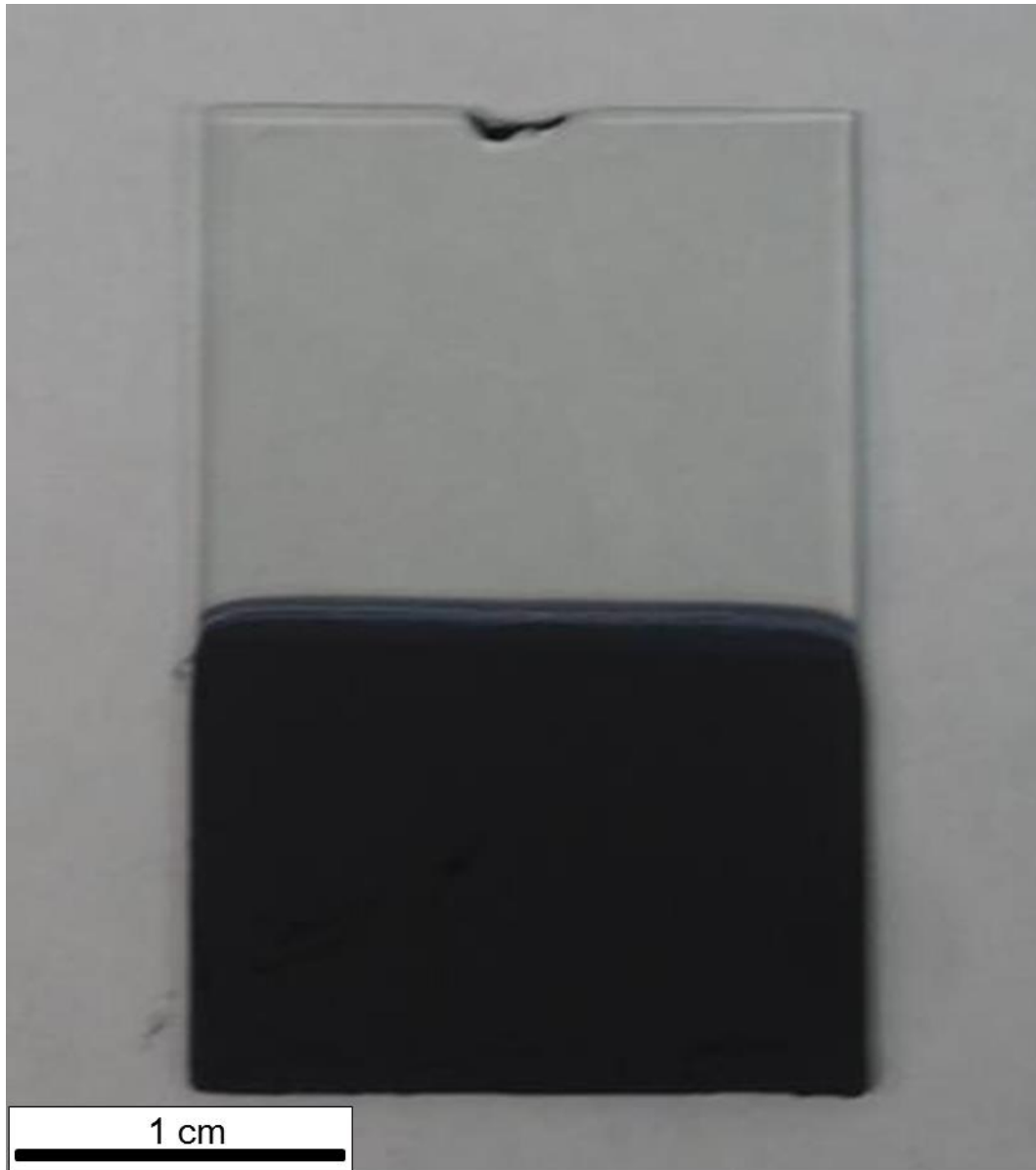


Fig. 2-4. Photograph of multilayered films with $(\text{Al}_2\text{O}_3/\text{NMC})_5$ structure on ITO glass prepared under constant voltage of 50 V.

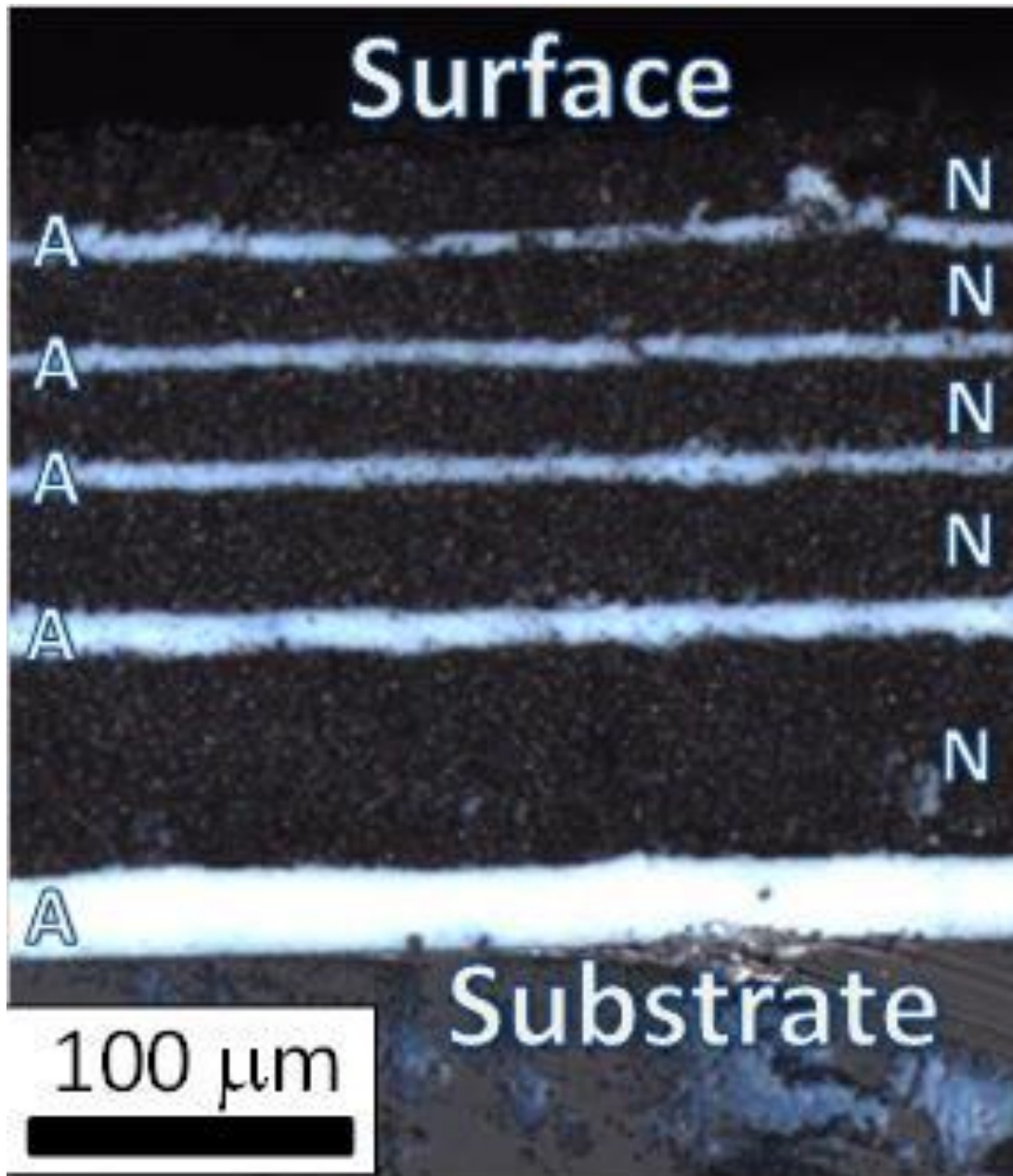


Fig. 2-5. Cross-sectional image of multilayered films with $(\text{Al}_2\text{O}_3|\text{NMC})_5$ structure on ITO glass fabricated by applied constant voltage of 50 V; where A denoted on white layers is Al_2O_3 ; N denoted on black layers is NMC.

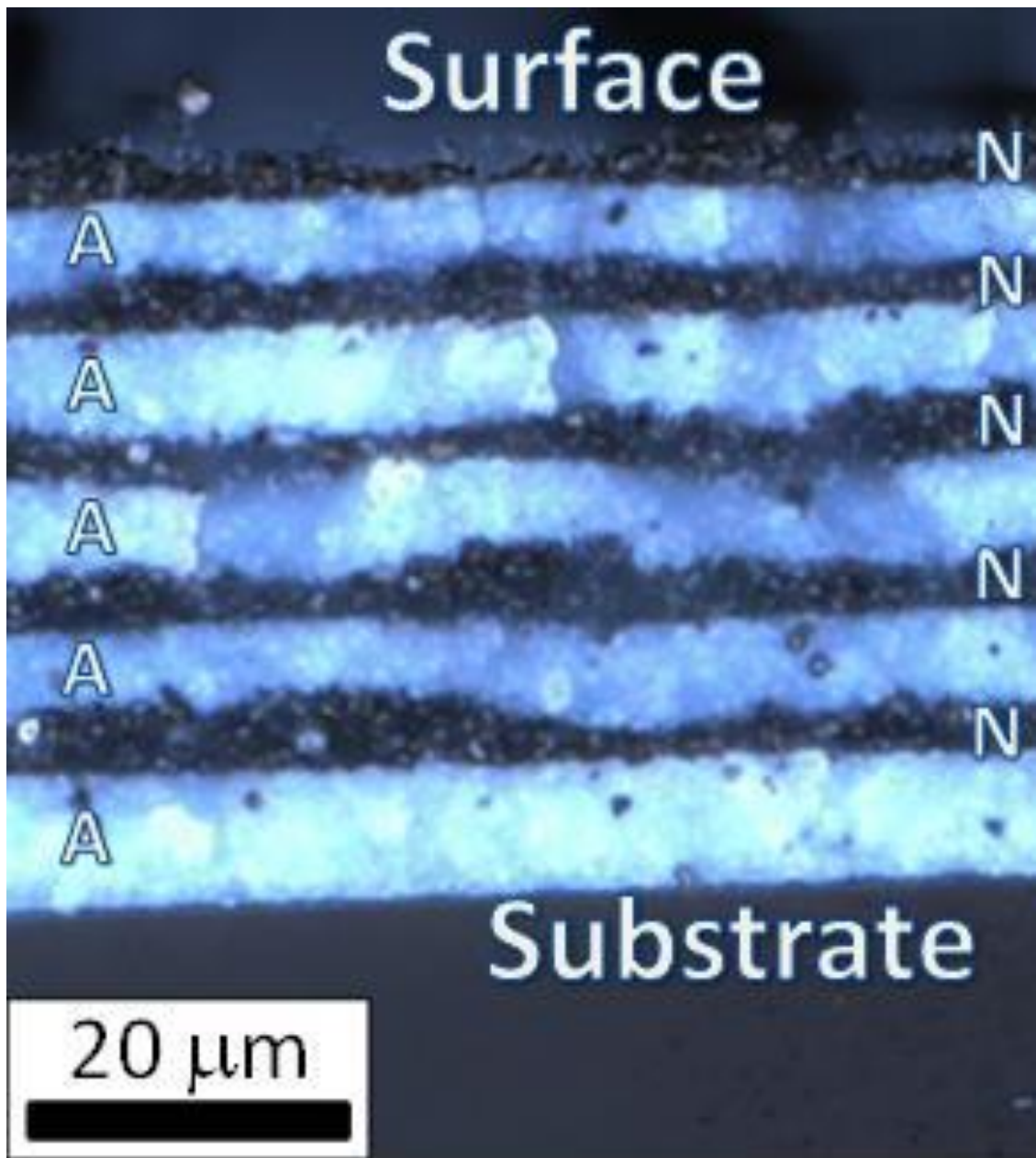


Fig. 2-6. Cross-sectional image of multilayered films with $(\text{Al}_2\text{O}_3|\text{NMC})_5$ structure on ITO glass fabricated by applied constant current density of $10 \mu\text{A cm}^{-2}$; Where A denoted on white layers are Al_2O_3 ; N on black layers are NMC.

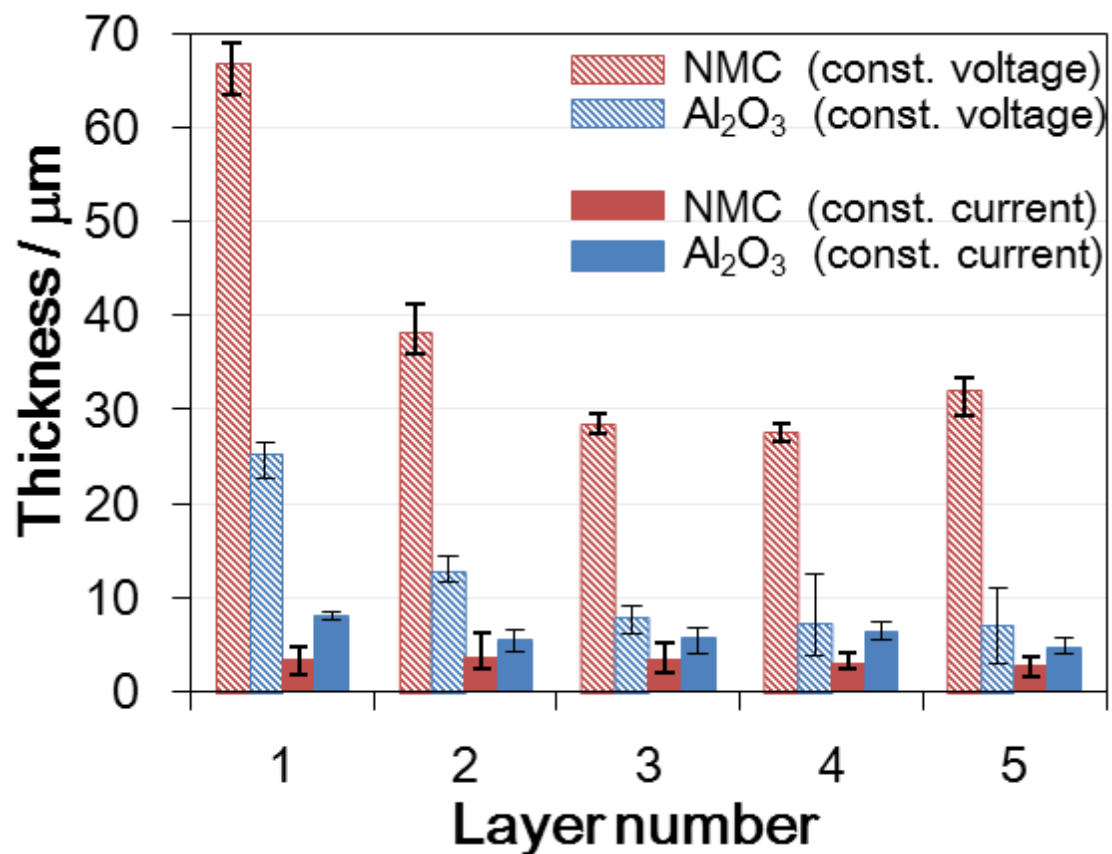


Fig. 2-7. Thickness of each layer in $(\text{Al}_2\text{O}_3|\text{NMC})_5$ films fabricated under applied constant voltage of 50 V and constant current density of $10 \mu\text{A cm}^{-2}$; where error bars indicate obtained maximum and minimum thickness in each number of layer.

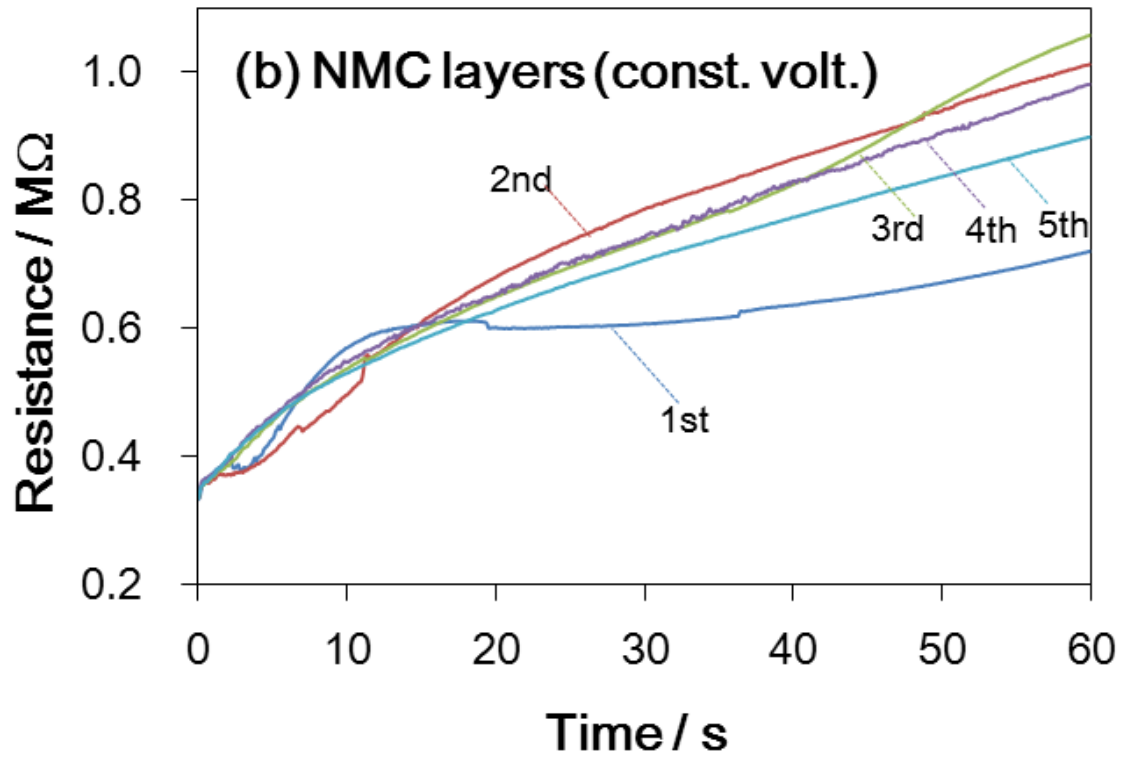
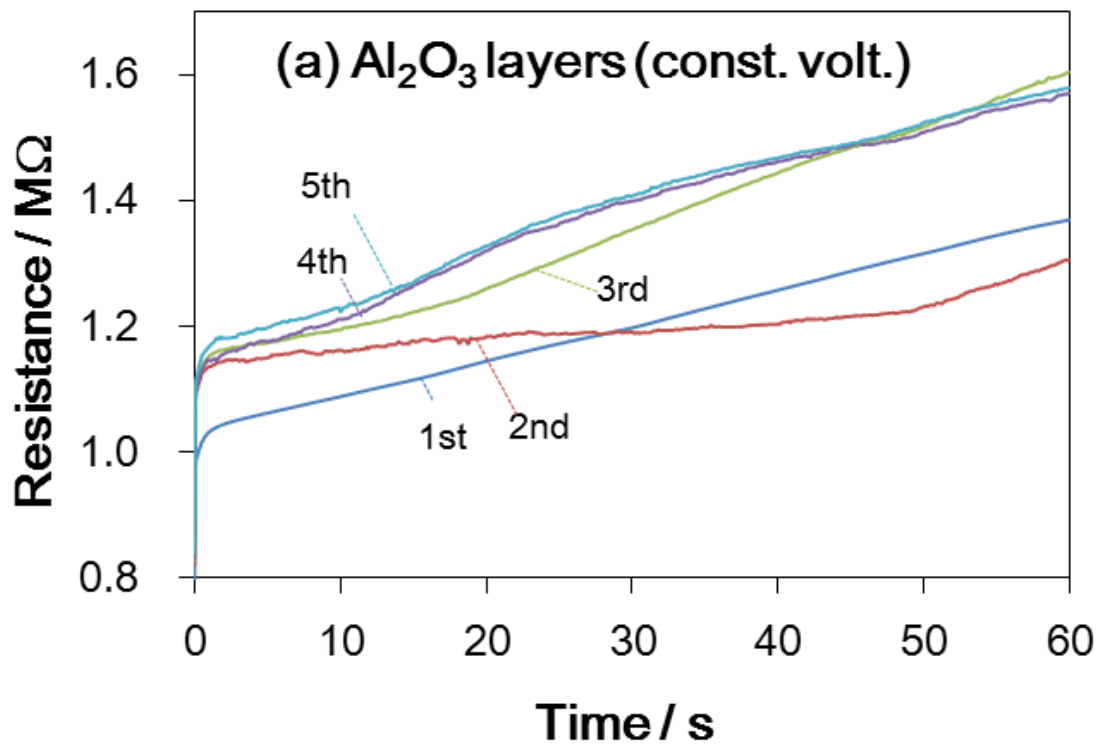


Fig. 2-8. Transitions of resistance for each layer with (a) Al₂O₃ and (b) NMC under applying constant voltage.

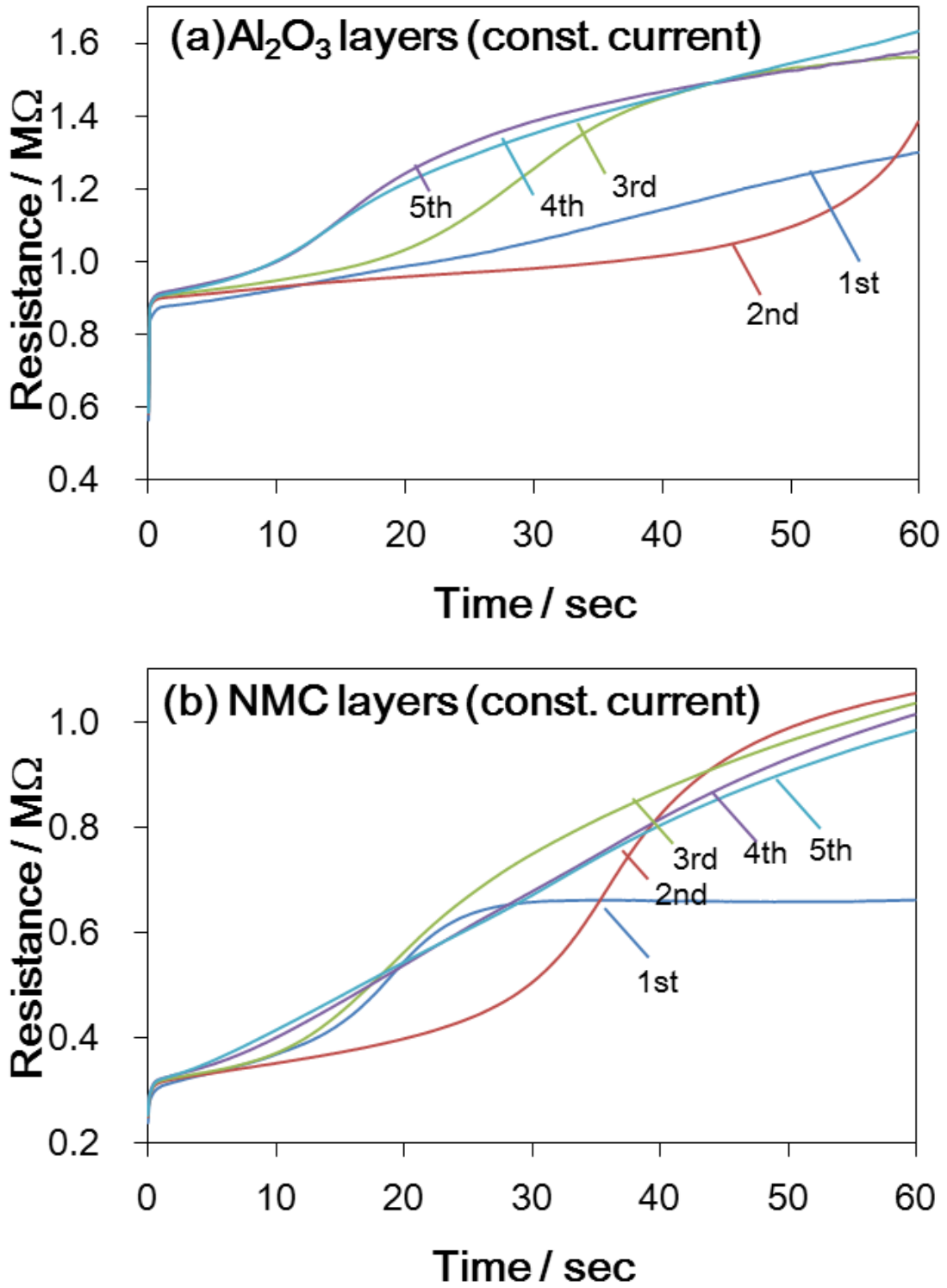


Fig. 2-9. Transitions of voltage for each layer with (a) Al₂O₃ and (b) NMC under applying constant current.

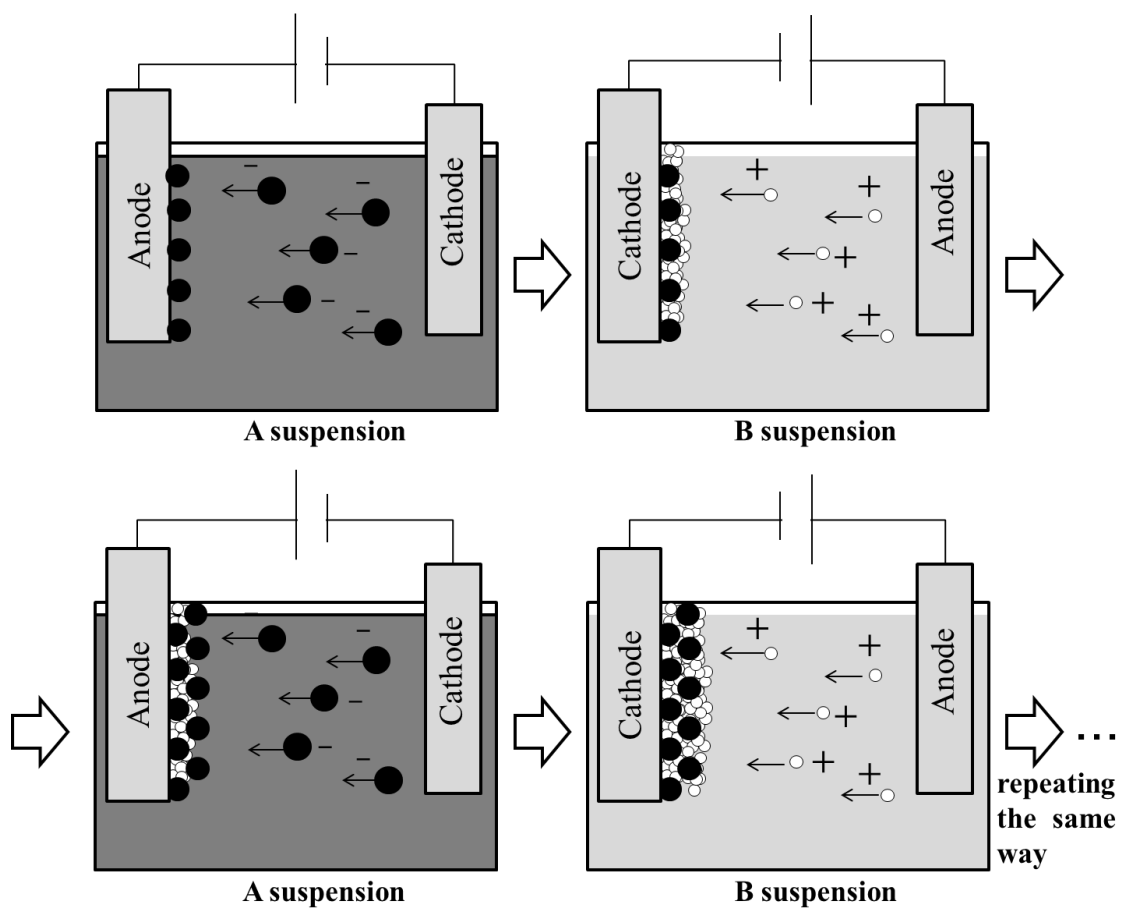


Fig. 2-10. Scheme of fabrication procedure for particle-reinforced composite films using EPD.

Chapter III

Investigation electrochemical performance and interfacial properties of photoelectrode based on NiTi-layered double hydroxide / reduced graphene oxide composite fabricated by electrophoretic deposition

3.1. Introduction

Global warming and the depletion of energy resources caused by the large-scale consumption of fossil fuels have become detrimental to the human race. Solar energy is an abundant source of renewable energy available to be harvested. To date, the cost of conventional solar power relative to fossil fuel alternatives has impeded its widespread use in grid-tied locations. One of the most efficient approaches is to use the solar energy in water splitting process to generate H₂ and O₂ molecules through photocatalysts. Photoelectrochemical cells (PEC) are solar cells that could generate electricity or hydrogen through electrolysis of water similar to Honda–Fujishima effect¹⁾. The photocatalyst used for the anode is one of the most important factors for the performance of PECs, which determines the generation of proton and electron by water photo-electro-oxidation. The most common photocatalysts used for PEC are TiO₂-based semiconductors due to its higher photocatalytic activity and robust water-splitting ability. However, the effectiveness is limited to ultra-violet light (UV) excitation, which only comprises of 3–5% of solar energy. This issue hinders the practical applications of photocatalysts in various fields. Therefore, novel and efficient visible-light driven photocatalysts are essential to meet the practical requirements of solar energy conversion.

Layered double hydroxides (LDHs), which are also known as hydrotalcite-like compounds, possess a layered structure of general formula [M(II)_{1-x} M(III)_x(OH)₂] [A_{x/n} H₂O], where M²⁺ and M³⁺ are divalent (Mg²⁺, Fe²⁺, Co²⁺, Cu²⁺, Ni²⁺, Zn²⁺) and trivalent (Al³⁺, Cr³⁺, In³⁺, Mn³⁺, Ga³⁺, Fe³⁺) metal

ions, respectively. A is an interlayer anion that could consist of the following (CO_3^{2-} , SO_4^{2-} , NO_3^- , F, Cl). LDHs also include a large class of important layered anionic clays. Interestingly, LDH-based photocatalysts, which possess both adsorption features and photocatalytic activity, were also reported in the literature for organic pollutants degradation²⁾ and for visible-light-induced O_2 and H_2 generation from water³⁾. Yeob Lee et al. reported the visible-light responsive photocatalytic behavior of NiTi-LDH under a co-existing sacrificial reduction reagent, such as AgNO_3 ⁴⁾. The visible-light responsiveness of NiTi-LDH was attributed to visible-light absorption during metal-to-metal charge transfer (MMCT) between Ni and Ti, influenced by the metal elements that have different valence in the LDH structure. Furthermore, NiTi-LDH exhibits efficient charge separation of photogenerated electron-hole pairs because of the high dispersion of TiO_6 units in the LDH structure⁵⁾. Recently, Bei Li et al. reported a NiTi-LDH/reduced graphene oxide (rGO) composite, which demonstrated photocatalytic water oxidation of approximately 7 times higher than that of WO_3 ⁶⁾. As above mentioned, NiTi-LDH is suitable for application as a photoanode-catalyst. Although investigations into the higher activity of NiTi-LDH materials have been performed, a photoanode based on the NiTi-LDH properties is rarely reported.

Electrophoretic deposition (EPD) method has been attracted attention as an easy preparation process for various type of film materials^{8,9)}. EPD is a unique coating technology categorized under colloidal process; under the influence of electric field, the charged colloids or particles suspension in a fluid are directed and deposited as thick films on the opposed charged electrodes. In utilizing this feature, films based on various functional materials were fabricated by EPD applying to electrochemical devices. Thus, film consisting of NiTi-LDH and its composite materials are probably prepared as photoanode by EPD. On the other hand, heterogeneous system such as photoanode shows highly sensitive in both their nanoscale and microscale structure, in different from homogeneous system such as suspensions

which is as general employing way of photocatalyst. Therefore, effects on performance of EPD films, based on NiTi-LDH and NiTi-LDH/rGO, and their electron dynamics due to difference of nanostructure should be investigated for enhancing performance of prepared materials.

In this work, as study case of performance evaluation of functional film with controlled nanostructure, NiTi-LDH/rGO composites have been synthesized by the co-precipitation method, and NiTi-LDH/rGO films were deposited by EPD on a fluorine-doped tin oxide (FTO) transparent conductive glass substrate. NiTi-LDH film-coated FTOs were systematically characterized, and their detailed electrochemical properties were evaluated and discussed for illustration of electron transport process in NiTi-LDH / rGO.

3.2. Experimental Procedure

3.2.1. Synthesis of NiTi-layered double hydroxide / reduced graphene oxide composite powder and its dispersion

Graphene oxide (GO) was synthesized from crystalline flake graphite as reported by Yuta Nishina⁹⁾. The GO suspension (0, 1.0, 2.0 wt.% of the NiTi-LDH catalyst) was prepared by sonication (Branson 2510, 30 min) of the GO powder in 100 mL of deionized water. Ni(NO₃)₂·6H₂O, TiCl₄ solution and 0.1 mol urea with Ni:Ti molar ratios of 4 were dissolved in the above GO suspension (TiCl₄ solution: 0.5 mL; the solution was prepared with a volume ratio of 1:1 from 0.002 mol TiCl₄ to concentrated hydrochloric acid [5]). After the solution was stirred vigorously for 24 h at a refluxing temperature (90 °C), the final precipitate was collected by centrifugation and rinsed thoroughly with an ethanol solution (1:1, v/v). The obtained product was dried in an oven at 60 °C for 24 h.

Then composite powder was coated with poly(diallyldimethylammonium chloride) (PDDA) by mixing the composite powder into PDDA aqueous solution. The PDDA-coated powder was added to a

30 vol.% ethanol aqueous solution for 5 mg mL^{-1} and was ultrasonicated (Branson 2510) for 30 min to obtain a NiTi-LDH/rGO dispersion.

3.2.2. Fabrication of NiTi-layered double hydroxide film coated electrode by electrophoretic deposition

The resulting NiTi-LDH and NiTi-LDH/rGO composite dispersions obtained were used as electrolyte in EPD process. FTO substrates were first cleaned using RCA method prior to be used for anode and cathode. EPDs of the NiTi-LDH/rGO composites were carried out at a current density of 0.2 mA cm^{-2} using a DC power supply. EPD time was divided into 5-s steps to prevent cracking of deposited film¹⁰. NiTi-LDH/graphene composite films were obtained on cathodic FTOs. The electrodes were fixed in parallel to each other with a distance of 1 cm. After EPD treatment, the EPD film-prepared FTO substrate was heated at 250°C for 30 min.

3.2.3. Characterization and evaluation of NiTi-layered double hydroxide film-coated electrodes

X-ray diffraction (XRD) of the NiTi-LDH/rGO film on FTOs was done using Rigaku Ultima IV diffractometer with a Cu $K\alpha$ source. Scan step of 0.02° and a scan range between 5° and 65° were used. The morphology of the films was investigated using a scanning electron microscope (SEM; S-4800, Hitachi) with an accelerating voltage of 10 kV. The photovoltages of NiTi-LDH/rGO composite films on FTO were measured under Xe lamp (HAL-320, Asahi Spectra, 1 kW m^{-2}) irradiation through potentiostat / galvanostat (SI1287, Toyo). A three electrodes system was used for the measurement with Pt wire, Ag/AgCl electrode and $0.5 \text{ M K}_2\text{SO}_4$ as the counter electrode, reference electrode and electrolyte, respectively. In order to determine the band edge potentials of the film, a Mott-Schottky plot was constructed from the capacitance data derived from the impedance fitting using an equivalent circuit and the frequency range explored was 100 mHz to 100 kHz. X-ray photoelectron spectra (XPS)

were recorded using a PHI Quantera SXM-CI X-ray photoelectron spectrometer equipped with a monochromatic Al K α X-ray source.

3.3. Results and discussion

3.3.1. Characterization of NiTi-layered double hydroxide / reduced graphene oxide composite powder and the composite film-coated electrodes

Fig. 3-1 (b) shows the XRD patterns of NiTi-LDH/rGO composite films on the FTO substrate. The basal diffraction peaks of meaning (003) and (006) are attributed to the hydrotalcite structure, which can be clearly observed at 12° and 24° in each sample despite different rGO content [5,6]. This result indicates that NiTi-LDH particles have been deposited on the FTO substrate by EPD without degradation. In addition, there was no non-basal diffraction peak in the XRD patterns. This suggests that the deposited LDH particles have a c-axis orientation owing to the applied electric field. Typical diffraction peaks of rGO were not observed in the NiTi-LDH/rGO composite, which can be attributed to either the superimposed characteristic reflection of rGO at 24° or low loading of rGO, which could be under the detection limit of XRD. The graphene existing in the composite was determined by Raman spectroscopic analysis which detected the typical peaks of graphene at 1584.6 and 1357.7 cm⁻¹ originating from the G and D bands, respectively (Fig. 3-3).

The surface and cross-section SEM images of the NiTi-LDH/*x* wt.% rGO films on FTO are shown in Fig. 3-2. A dense NiTi-LDH film was formed on the FTO glass substrate with thickness of approximately 10 μ m. The thickness increment of the composite films was observed with longer total EPD time. By comparing both NiTi-LDH films with and without rGO, the difference in film roughness can be observed. The approximate ratio of particles in parallel to the FTO substrate was calculated from the surface SEM images of the samples containing 0, 1.0 and 2.0 wt.% rGO as 50, 80 and 78%,

respectively. The differences in the density and c-axis orientation caused by the dispersity have consequently affected the final morphology of the rGO incorporated films.

3.3.2. Evaluation of electrochemical performance and interfacial properties of NiTi-layered double hydroxide / reduced graphene oxide in photoelectrochemical systems

Fig. 3-4 shows the transient photovoltage of the NiTi-LDH/*x* wt.% film-prepared FTO electrode under Xe lamp irradiation. NiTi-LDH films with 1.0 and 2.0 wt.% rGO were observed to exhibit a higher photovoltage and increment rate compared to those of the NiTi-LDH film without rGO. The parameters of the prepared films are obtained from the transient photovoltage and are provided in Table 3-1. The fitting of Eq. (3-1) from 10 ~ 80 s using least square method is to determine the photogeneration rate (*G*) and relaxing time (τ) upon Xe lamp irradiation at 10 s to the highest photovoltage (V_{ph}) saturated at around 80 s as represented in Fig. 3-4.

$$dV(t) / dt = G - V(t) / \tau \quad (\text{Eq. 3-1})$$

Where *V* is the current photovoltage at a certain time (*t*). The highest V_{ph} was obtained in the film containing 1.0 wt.% rGO. The increasing value of *G* with increasing rGO content suggests that rGO addition increased the probability of charge-separation of the generated electron-hole pair in the NiTi-LDH photocatalyst. The improving V_{ph} with rGO addition is explained by the increasing *G*. Generally, the lifetime of an excited electron in the photocatalyst tends to be longer when the efficiency of charge-separation is enhanced, which means that the photovoltage of the photoelectrode is improved. However, the sample with 2.0 wt.% rGO did not exhibit the best performance despite having a higher *G* compared with the 1.0 wt.% sample and τ , referring to the lifetime of the excited electron, is reduced despite larger content of rGO. From Eq. (3-1), in order to achieve a higher V_{ph} , it is

necessary to improve both parameters, G and z . Thus, NiTi-LDH with 1wt.% rGO can be determined as best component in this work. Additionally, it was observed that conflicting effects for V_{ph} are introduced by compositing with rGO.

For in-depth analysis, electrochemical impedance spectroscopy (EIS) was employed for the evaluation of the band structure and interfacial recombination kinetics in NiTi-LDH/rGO composite films. Fig. 3-5 and Table 3-2 show the Mott-Schottky plots and parameters for the NiTi-LDH/ x wt.% rGO films, respectively. The parameters were calculated by Eq. (3-2).

$$C^{-1} = 2 (E - E_{fb}) / eN_C \varepsilon \varepsilon_0 \quad (\text{Eq.3-2})$$

Where C is the capacitance (F), E is the applied potential (V vs. SHE), E_{fb} is the flat band potential (V vs. SHE), e is the electron charge (C), N_C is the carrier density (cm^{-3}), ε is the specific induction of sample, and ε_0 is the vacuum dielectric constant (F m^{-1}). One of the factors for V_{ph} alteration is the difference of band structure, especially the flat band potential. In this experiment, there was no significant variation of the plots or the parameters obtained from each of the composite films containing x wt.% rGO. Therefore, we can estimate that the main factor for altering V_{ph} and the associated parameters contribute to the kinetic behavior, i.e., the charge transfer on the interface.

EIS is performed to investigate the dynamics of the interfacial charge transfer process in a NiTi-LDH/rGO film-prepared electrode. Fig. 3-6 shows the Cole–Cole plots for the photoanode based on unmodified and rGO-modified NiTi-LDH at -0.55 V bias in the dark. In this case, only the charge transfer related to the recombination reaction occurs, consequently the photoanode maintains an open-circuit voltage because of the applied bias potential¹¹⁾. The Cole–Cole plots show an irregular semicircle with a different radius. These results indicate that the photoanode-prepared composite film has two kinds of resistance components under the flat band state and these resistances are influenced

by combining with rGO. For estimating the parameters of the electrochemical reaction at the interface, an equivalent circuit which is illustrated in Fig. 3-7 was employed to enable fitting analysis of the Cole–Cole plots. The resulting parameters obtained by the fitting analysis are shown in Table 3-3, where R_s is the series resistance (not included in Table 3-3); R_{se} is the resistance ($k\Omega$) of charge transfer through the semiconductor film; R_{rec} is the recombination resistance ($k\Omega$) at the electrode/electrolyte interface; C_μ (μF) is the chemical capacitance obtained from CPE, the mean of C_μ is the capacitance of an accumulated electron in NiTi-LDH/rGO; τ_{rec} is the lifetime (ms) of the excited electron calculated by Eq. (3-3).

$$\tau_{rec} = R_{rec} C_\mu / 2\pi \quad (\text{Eq. 3-3})$$

As shown in Table 3-3, R_{sc} , R_{rec} , and τ_{rec} decreased with increasing rGO content due to the acceleration of the recombination reaction between the electron-hole pair at the electrode/electrolyte interface. These degraded parameters corroborate the fall-off of τ shown in Table 3-1. In contrast, an increase of C_μ is observed with increasing rGO content. B. Li et al. reported that Ti^{3+} levels, which relate to defects in the chemical structure of NiTi-LDH, are increased by compositing with rGO [6]. Additionally, Y. Zhao et al. found two different forms of defects in NiTi-LDH: Ti^{3+} surface defects facilitate charge-separation by acting as a trap site for the excited electron and also as a reaction site for recombination; defects in the bulk only behave as a reaction site for recombination [5,12]. According to these reports, we can speculate that an increased C_μ indicates a higher amount of Ti^{3+} surface defects. Actually, the reduction of Ti $2p_{3/2}$ in NiTi-LDHs could be observed from peak tailing toward low binding energy (Fig. 3-8 (a)), which was associated with increasing of Ti^{3+} ratio, i.e. 4.34, 5.04 and 5.79% when the addition amount of rGO was 0, 1.0 and 2.0 wt.% respectively (Fig. 3-8 (b)). Furthermore, the reason for varying G , τ , R_{sc} , R_{rec} and τ_{rec} values can be explained by monitoring the

Ti³⁺ levels on the charge-transfer dynamics in the NiTi-LDH/rGO composite. Fig. 3-9 shows a schematic of the mechanism of the changing photoelectrochemical properties in NiTi-LDH by compositing with rGO. Based on the assumption that there is no difference in the roles between pristine and new Ti³⁺ levels generated with rGO, we can estimate the following:

1. New Ti³⁺ and rGO levels are generated by compositing with rGO during synthesis of the NiTi-LDH/rGO composite.
2. Charge separation of the electron-hole pair generated in the bulk of NiTi-LDH is enhanced by the increased Ti³⁺ defects and rGO levels.
3. However, the recombination reaction acceleration resulted resulting in an increase of reaction sites, i.e., Ti³⁺ surface defects.

In summary, the rates of the charge separation and recombination reactions are dependent on the number of reaction sites. In terms of the two conflicting reactions, the charge separation rate is dominant compared with the recombination rate by the introduction of rGO. Consequently, the V_{ph} of the electrode prepared with NiTi-LDH / rGO composite film is improved.

3. 4. Conclusion

As study case of performance evaluation of functional film, with controlled nanostructure, NiTi-LDH/rGO films with thickness of approximately 2–14 μm were prepared on FTO by the EPD method. In addition, the films obtained were dense with certain level of orientation due to the introduction of rGO. The NiTi-LDH/rGO|FTO showed a higher photovoltage compared to that of pristine NiTi-LDH|FTO. The highest V_{ph} was obtained in the film containing 1.0 wt.% rGO. Kinetic parameters were obtained by fitting analysis of the transient photovoltage and Cole–Cole plots. From our analysis, it was found that a conflicting effect where two opposing reaction rates for V_{ph} are

introduced by compositing with rGO. Consequently, the V_{ph} of the electrode prepared with a NiTi-LDH/rGO composite film is improved. The expected effects due to the nanocomposite structure were also observed substantially in the performance of the composites-based EPD films employed as photoanode, which showed highly sensitive in both their nanoscale and microscale structure.

References

- 1) M. Grätzel, *Nature*, **414**, p. 338 (2001).
- 2) L. Mohapatra and K.M. Parida, *Sep. Purif. T.*, **3**, p. 73 (2012).
- 3) C. G. Silva , Y. Bouizi , V. Fornés and H. García, *J. Am. Chem. Soc.*, **131**, p. 13833 (2009).
- 4) Y. Lee, J. H. Choi, H. J. Jeon, K. M. Choi, J. W. Lee and J. K. Kang, *Energy Environ. Sci.*, **4**, p. 914 (2011).
- 5) Y. Zhao, P. Chen, B. Zhang, D. S. Su, S. Zhang, L. Tian, J. Lu, Z. Li, X. Cao, B. Wang, M. Wei, D. G. Evans and X. Duan, *Chem. Eur. J.*, **18**, p. 11949 (2012).
- 6) B. Li, Y. Zhao, S. Zhang, W. Gao and M. Wei, *Appl. Mater. Interfaces*, **5**, p. 10233 (2013).
- 7) L. Besra and M. Liu, *Prog. Mater. Sci.*, **52**, 1-61 (2007).
- 8) T. Uchikochi, *Micromeritics*, **57**, 36-42 (2014).
- 9) Y. Nishina, *Japan Patent Kokai*, 2012-83453 (2012.12.12).
- 10) M. Hamadani and H. Sayahi, *J. Mater. Sci.*, **47**, p. 5845 (2012).
- 11) X. Luan, L. Chen, J. Zhang, G. Qu, J. C. Flake and Y. Wang, *Electrochim. Acta*, **111**, p. 216 (2013).
- 12) Y. Zhao, B. Li, Q. Wang, W. Gao, C. J. Wang, M. Wei, D. G. Evans, X. Duan and D. O'Hare, *Chem. Sci.*, **5**, p. 951 (2014).

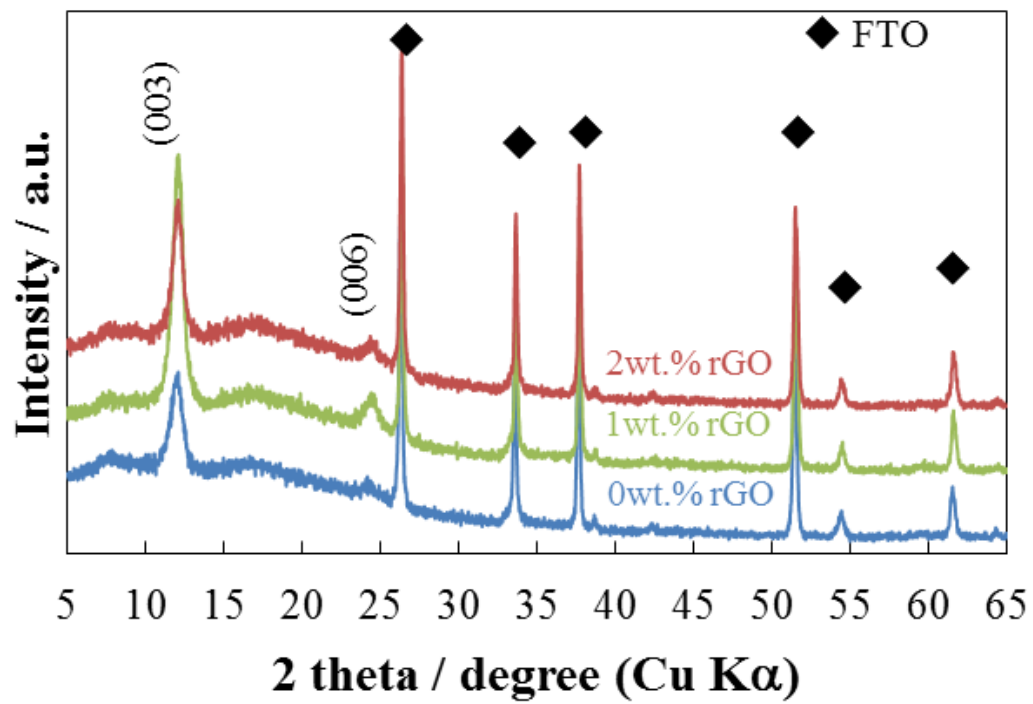


Fig. 3-1. X-ray diffraction patterns of NiTi-LDH / x wt.% rGO|FTO electrodes fabricated by EPD.

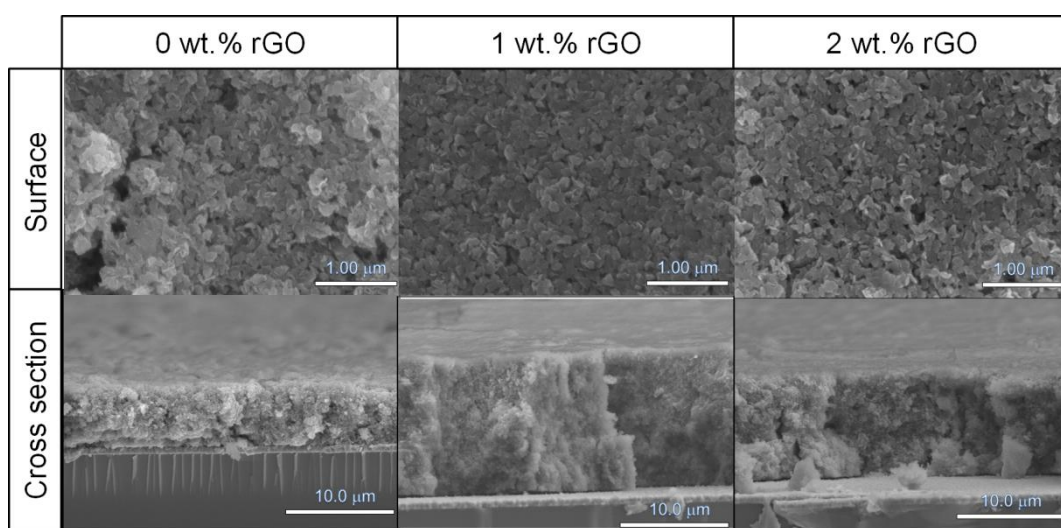


Fig. 3-2. SEM images of NiTi-LDH/x wt.% rGO|FTO cross section and surface fabricated by EPD.

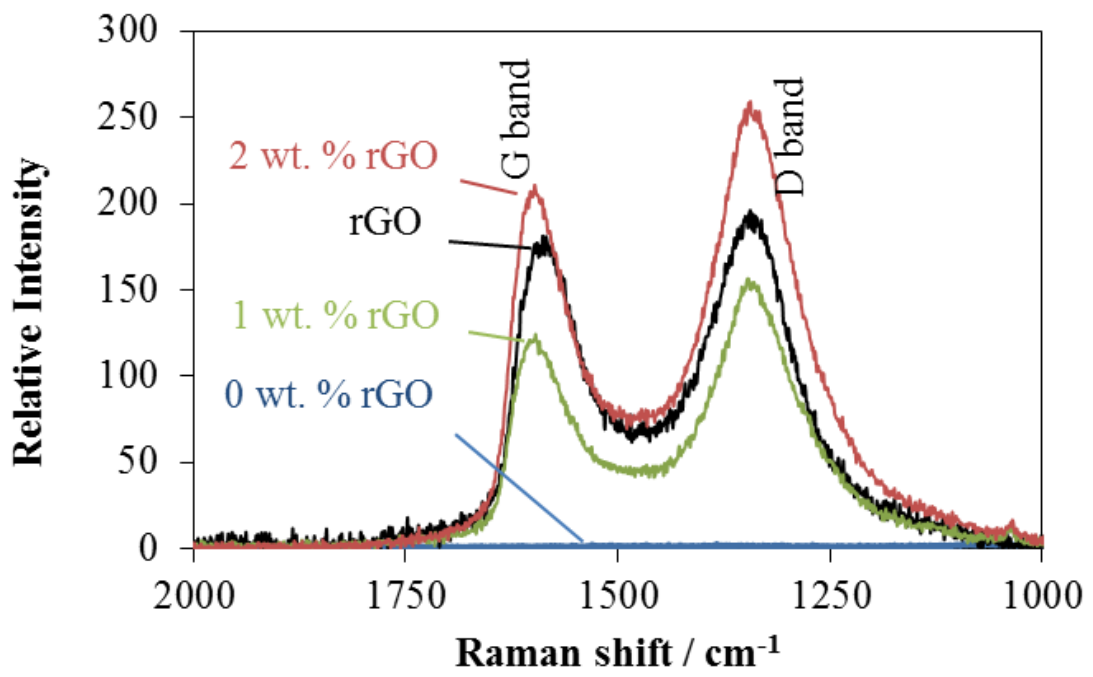


Fig. 3-3. Raman spectra of NiTi-LDH with various content of rGO. The spectrum of rGO is for reference.

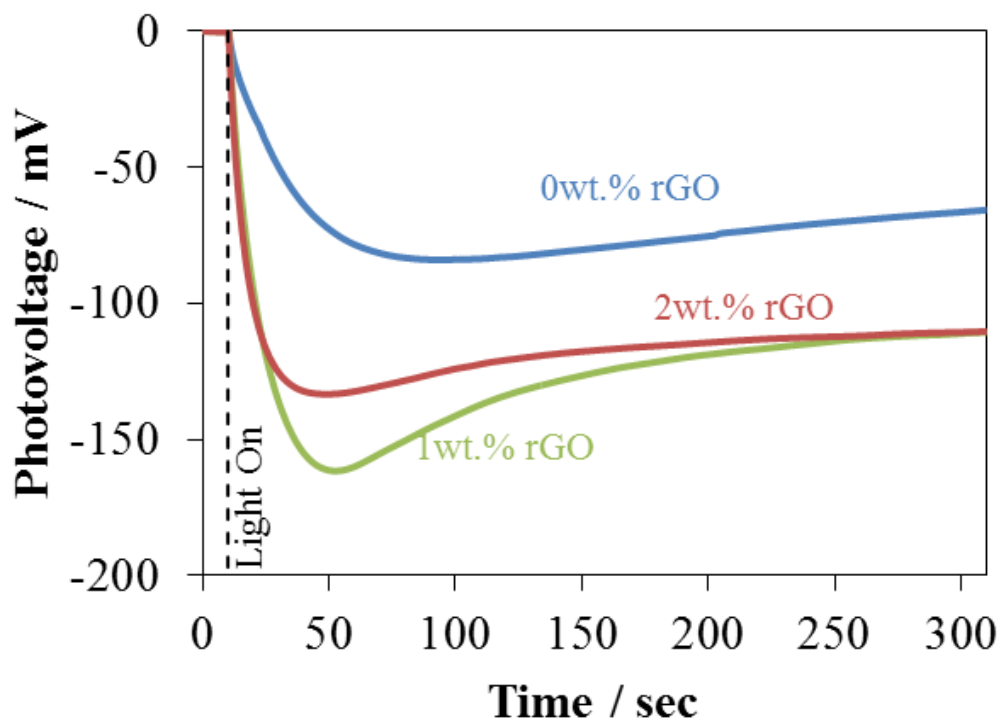


Fig. 3-4. Transition of the photovoltage of the NiTi-LDH/*x* wt.% rGO films modified on FTO fabricated by the EPD method in 0.5 M Na₂SO₄ purged by N₂ at 298 K under visible light (1 kW m⁻²) irradiation.

Table 3-1. Parameters of NiTi-LDH/rGO obtained from Fig. 3-4 using Eq. (3-1)

rGO ratio / wt.%	0	1	2
V_{ph} / mV	84.0	161.6	133.4
G / mV sec ⁻¹	3.79	14.39	18.64
τ / s	23.18	11.62	7.19

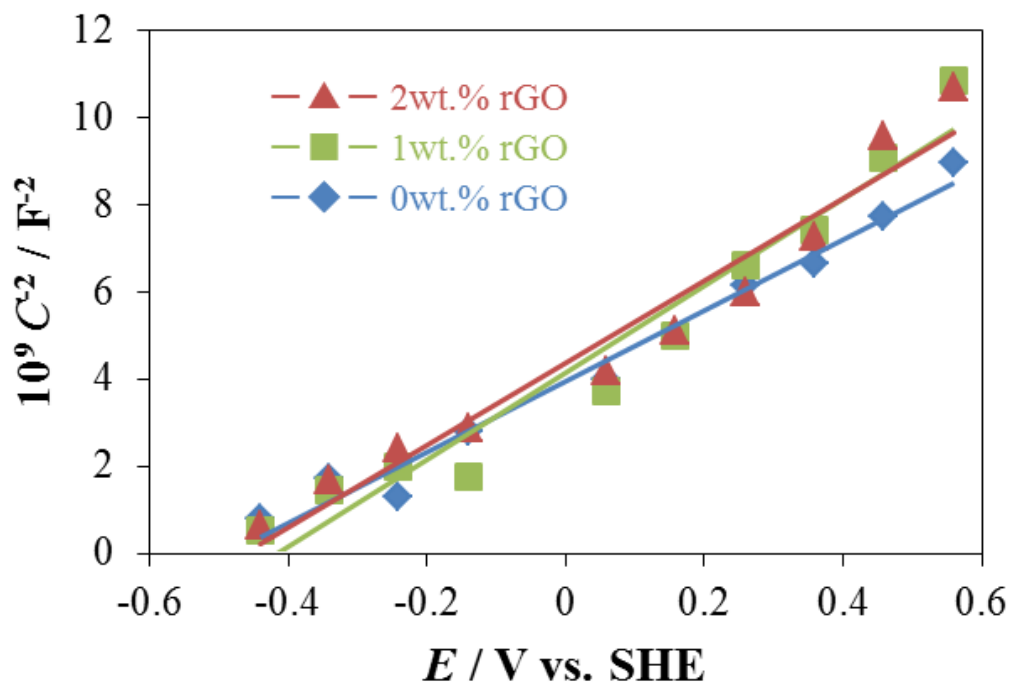


Fig. 3-5. The Mott-Schottky plots for the NiTi-LDH/ x wt.% rGO films modified on FTO fabricated by the EPD method in 0.5 M Na_2SO_4 purged by N_2 at 298 K under visible light (1 kW m^{-2}) irradiation.

Table 3-2. Parameters of NiTi-LDH/rGO obtained from Mott-Schottky plots.

rGO ratio / wt. %	0	1	2
E_{fb} / V vs. SHE	- 0.49	- 0.42	- 0.46
$10^{17} N_D$ / cm^{-3}	7.28	4.09	7.19

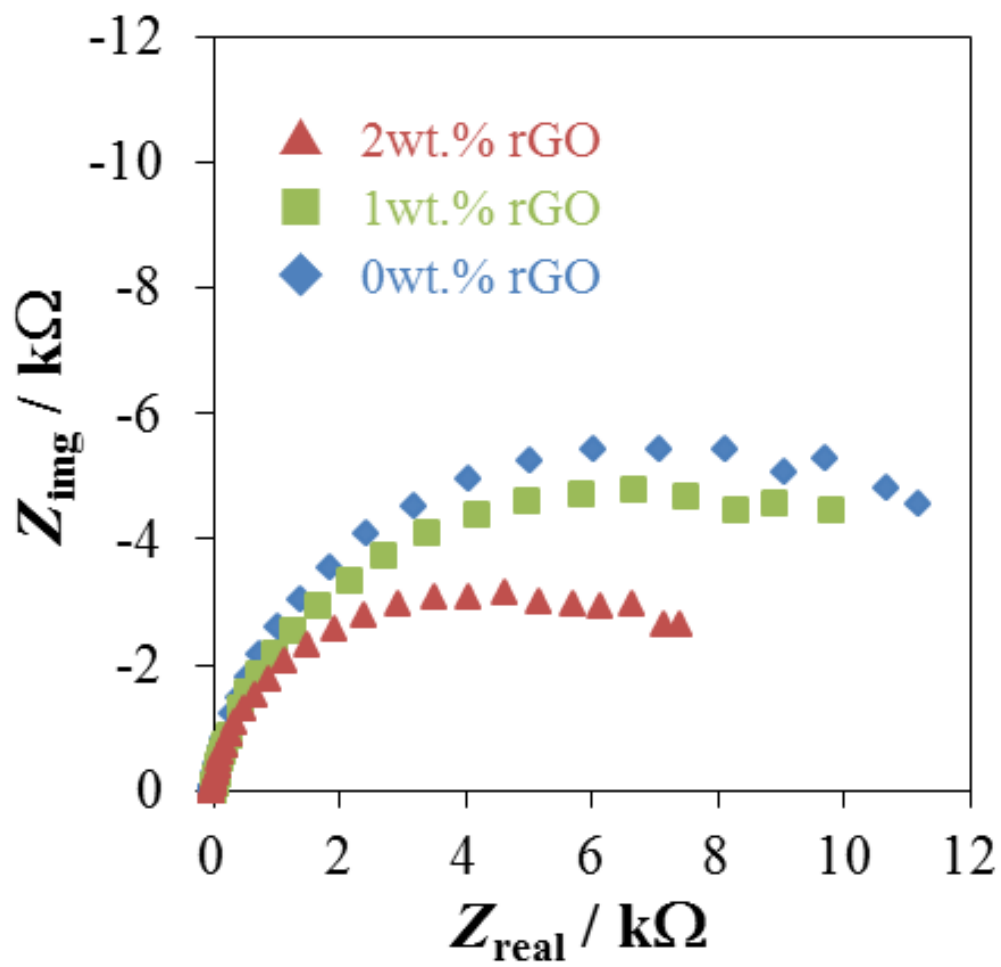


Fig. 3-6. Cole–Cole plots of the NiTi-LDH/*x* wt.% rGO films modified on FTO fabricated by the EPD method in 0.5 M Na₂SO₄ purged by N₂ at 298 K in the dark. The applied bias potential was -0.55 V vs. SHE.

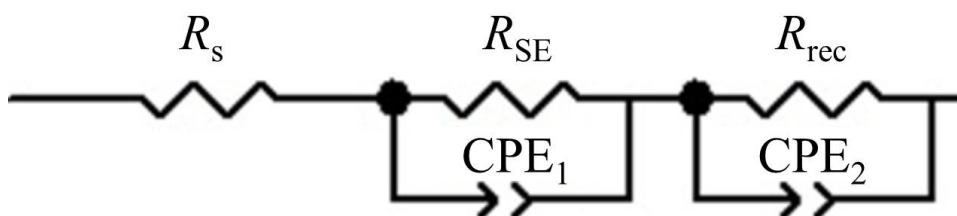


Fig. 3-7. Equivalent circuit of the photoanode for fitting analysis of the Cole–Cole plots in Fig. 3-4.

Table 3-3. Parameters of NiTi-LDH/rGO obtained by equivalent circuit fitting.

rGO ratio / wt.%	0	1	2
R_{SC} / $k\Omega$	6.94	7.08	5.15
R_{rec} / $k\Omega$	9.75	6.64	4.29
C_{μ} / μF	158	226	273
τ_{rec} / ms	245	239	186

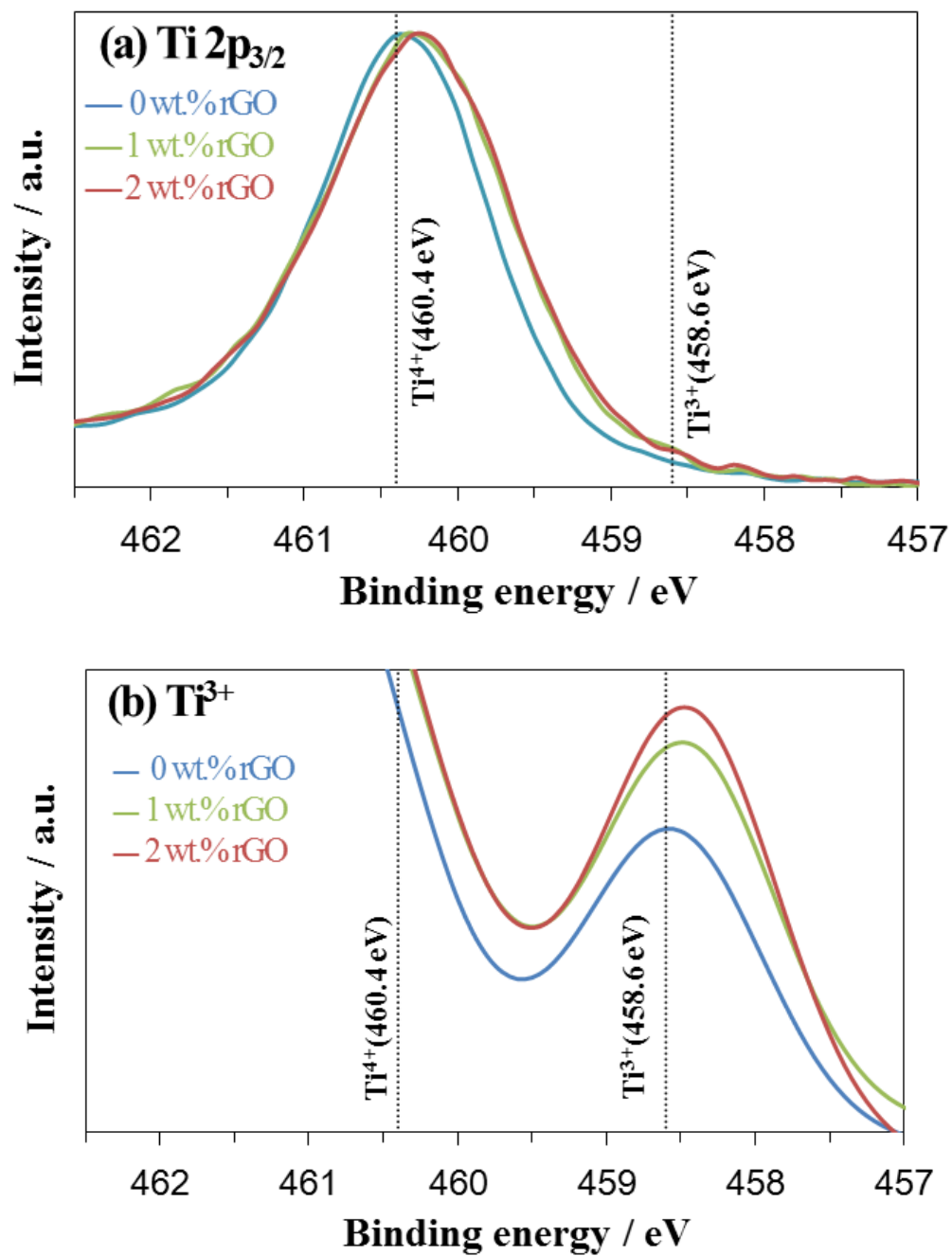


Fig. 3-8. XPS spectra of (a) Ti 2p_{3/2} and (b) separated Ti³⁺ peaks in NiTi-LDHs with various content of rGO.

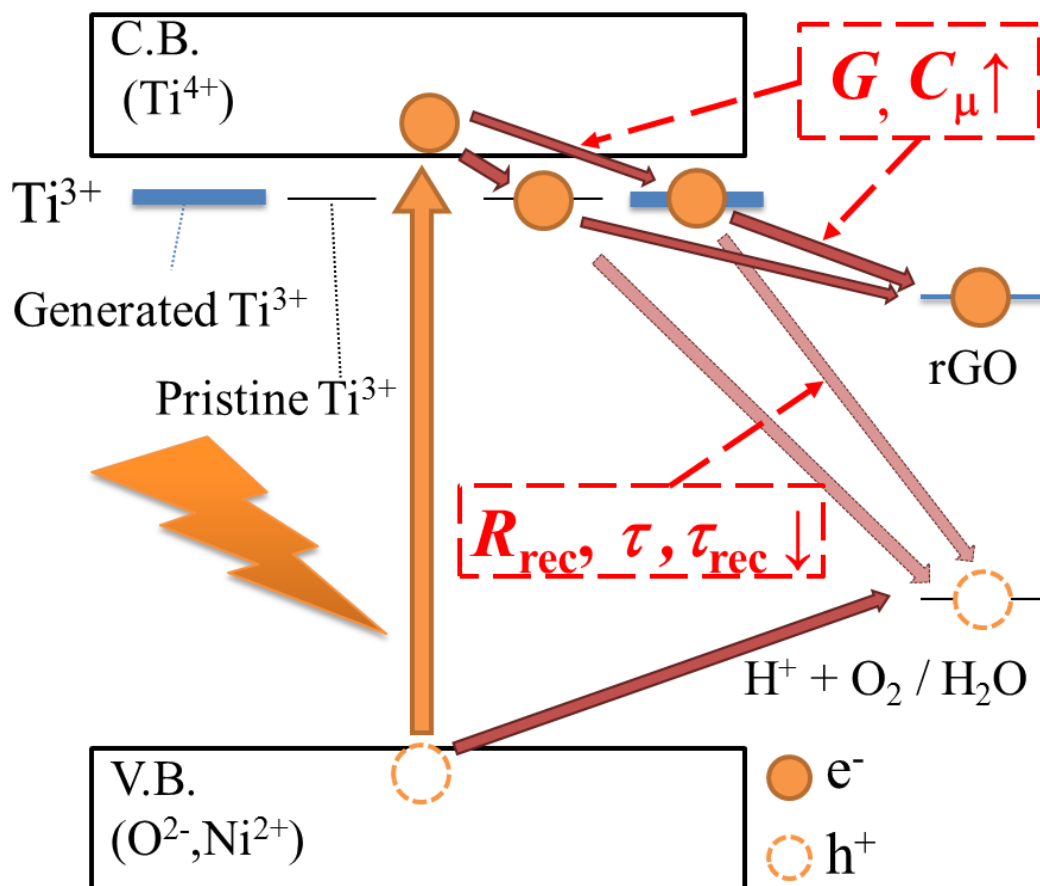


Fig. 3-9. Mechanism of changing photoelectrochemical properties in NiTi-LDH by compositing with rGO.

Chapter IV

Colloidal processing of $\text{Li}_2\text{S-P}_2\text{S}_5$ films fabricated via electrophoretic deposition and its characterization as solid electrolyte for all solid state lithium ion batteries

4.1. Introduction

Lithium ion batteries (LIBs) possess high voltage and high energy density and are valuable for portable devices as utilized widely used as power sources. Research activity into LIBs with high capacity, by upscaling and enhancing energy density, has increased dramatically in recent years for expanding application areas such as in electric-automobile and smart-grid systems ¹⁾.

Nearly all commercially available LIBs utilize liquid electrolytes as the medium for ion transport. These devices are capable of impressive performance but are inherently dangerous due to the flammability of the electrolytes used and the potential for environmental harm resulting from accidental leakage. These points necessitate special safety precautions in device packaging. All-solid-state LIBs, in which liquid organic electrolytes are replaced with solid-state-inorganic electrolytes, are expected to be the optimal rechargeable batteries in the next generation because of their higher energy density, cycle stability, and ignition safety. As solid electrolytes for novel solid-state LIBs, the sulfide-based lithium ion conductors are highly promising due to their high conductivities, single-ion conductive properties, and non-flammability. Mizuno et al. fabricated novel sulfide lithium-ion conducting materials, as $\text{Li}_2\text{S-P}_2\text{S}_5$ (LPS), with high conductivity at ambient temperature by a mechanical milling method ^{2), 3)}. Conventionally, mechanical milling is employed for preparing solid electrolytes, as mixtures of active materials and electron-conductive materials. However, by mechanical milling, it is difficult to control the distribution of the components in the mixture. In addition, mechanical milling method is not suitable for practical industrial manufacturing application because it is a time-consuming and energy intensive process. Thus, development of novel methods for preparation LPS that would involve low time and energy consumption, and with a wide versatility in its application is needed.

We previously reported that a suspension of LPS precursor (LPS-p) was successfully prepared using liquid-phase shaking (LS) method ⁴⁾. In this method, LPS is obtained within a relatively short time and with small energy consumption, using LPS-p suspension in ester solvents. Moreover, LS method is suitable for preparing homogeneous electrolytes, mixtures and the preparation of composite layers, based on its feature of dispersing components into the liquid phase. Processing to obtain electrolytes or composite layers directly from the suspensions is necessary to achieve above mentioned advantages, as a simple process for advanced film morphology control. Conventionally, LPS-p was recovered as the powder from suspensions, and electrolyte and composite were fabricated via solid phase eventually in current LS method; briefly, application of LPS-p suspension to direct colloidal processing was not developed yet.

Electrophoretic deposition (EPD) is an important technology for colloidal coating processes ⁵⁾. Under the influence of electric field, the charged colloids or particles suspended or dispersed in a fluid are moved towards and deposited on oppositely charged electrodes. In other words, any materials can be deposited on any charged substrates by EPD if a surface charge can be generated on the material dispersed in a solvent. The EPD technique with a wide range of novel application has recently gained increasing interest in the processing of advanced ceramic materials and coatings both in academia and the industrial sector. This increasing interest is because of not only the high versatility of its use with different materials and their different combinations but also because of its cost-effectiveness and requiring simple apparatus. Furthermore, morphology and microstructure of obtained films can be controlled easily and controlling the processing conditions such as strength of the electric field, applied time, wave shape, dispersion state, and sequence of deposition. Numerous applications of EPD have been developed for the fabrication of ceramics, including the preparation of coatings, fiber-reinforced composites, laminated materials, porous membranes, stepwise functionally graded materials and continuously graded materials. LPS films with desired morphology and microstructure, mentioned above, could be obtained via colloidal

processing of LPS particles by EPD. Incidentally, LPS can't be dispersed in polar solvents such as water and alcohol, which are the common dispersion media in EPD, because of the high reactivity of LPS with polar media. Hence, processing of LPS by EPD is limited to only in non-polar solvents. On the other hand, generating the surface charge on polar materials such as LPS in non-polar solvents is very difficult. For these reasons, there is need for research into the possibility of preparing LPS via EPD in non-polar solvents.

In this study, LPS films were prepared via EPD from suspension of LPS-p fabricated by LS method as a novel colloidal process and the characteristics of the films as a lithium ion conductor were evaluated.

4.2. Experimental

4.2.1. Preparation of suspension of Li_3PS_4 precursor

Li_2S and P_2S_5 were purchased from Mitsuwa and Merck respectively. Ethyl propionate (EP) and 3A molecular sieves were obtained from Sigma-Aldrich. The EP was dehydrated by 3A molecular sieves before used. Li_2S (0.3827 g), P_2S_5 (0.6173 g) [molar ratio $\text{Li}_2\text{S} : \text{P}_2\text{S}_5 = 3 : 1$], EP (10 mL) and zirconia balls (diameter 4 mm, about 32 g) were mixed and shaken at an amplitude of about 1 cm at 1500 rpm in a dry Ar atmosphere at 30°C for 6 h. The obtained suspension of LPS-p was diluted 10 times with EP and used as the deposition bath in an EPD process. As the reference in comparison of fabricating suspension, LPS glass powders (LPS-M) were prepared by mechanochemical milling method²⁾.

4.2.2. Deposition of Li_3PS_4 films from Li_3PS_4 precursor films via electrophoretic deposition

LPS-p was deposited on indium-doped tin oxide (ITO) glass substrates (40 × 20 × 5 mm) separated by a distance 0.5 cm for characterization. Constant voltage/current was supplied by source measure unit (GS610, Yokogawa). LPS-p film was treated by the conventional process according to the previous study⁴⁾ for converting to LPS film; specimens were heated at 170°C under vacuum (about – 100 kPa) for 2 h.

4.2.3. Characterization of electrophoretic deposition films

X-ray diffraction (Ultima IV, Rigaku) with CuK α radiation and Raman spectroscopy (NRS-3100, Jasco) with a green laser (wavelength: 532 nm) of the deposited LPS films were carried out to identify crystalline phases and local structure. The morphology of the deposited films was investigated using scanning electron microscopy (SEM) (S4800, Hitachi).

The scheme of the cell for AC impedance measurement is illustrated in Fig. 4-1. The two Al substrates (\varnothing 10 \times 5 mm) deposited with the LPS-p film were prepared by EPD with the same condition mentioned above; employing two specimens is for preventing the short circuit between SUS plugs due to too thin LPS film obtained after press process mentioned follows. Heat aging of the resultant LPS-p films was carried out via the two ways; treated by conventional condition denoted above; warm pressed at 220°C with the pressure of 30 MPa under air pressure for 1h before conventional aging. All film specimens were uniaxial-pressed using SUS plugs, which have roles as presser and electrode, at the pressure of 330 MPa for 1 min followed by heat age treatment. Employing the cells prepared by according to above procedure, the ionic conductivity was evaluated using an AC impedance measurement analyzer (SI1260, Solatron), from 1 MHz to 10 Hz in a dry Ar flow atmosphere. As the reference, pelletized LPS was prepared by pressing of LPS powder (80 mg) obtained from LS method at the pressure of 330 MPa.

4.3. Results and discussion

4.3.1. Evaluating of dispersion state of Li₃PS₄ precursor in nonpolar-solvent for applied to electrophoretic deposition

Fig. 4-2 illustrates the photographs of the (a) LPS-M and (b) LPS-p suspensions. The sediment of LPS-M in EP was observed shortly after sonication. It is well known that polar-matters such as LPS can't be dispersed in the non-polar solvent such as EP because of their non-affinity. On the other hand, the freshly prepared LPS-p precursor suspension after sonication was stable for several hours which indicated

that LPS-p precursor already has dispersibility in EP without any treatment or additives. This stability may be originated from the structure of LPS-p precursor which contained both LPS and EP in its structure. It is also confirmed that LPS-p powder obtained after drying at elevated temperature, i.e. 170°C, couldn't be re-dispersed into EP solvent, similar to the result from LPS-M. Thus, direct application of the as-prepared suspension is better for possibility of achieving EPD and the procedure is also simple. Fig. 4-3 shows the current curves obtained from different suspensions under constant applied voltage (100 V / 0.5 cm) between ITO substrates for 60 s. Almost no current was observed in EP without LPS and LPS-p obviously during applying the voltage by reason that EP is non-polar and not included any polar-matters. By contrast, high current density was observed in EP suspended with LPS-p in the process. It means that LPS-p exhibits ionic dissociation in EP, and dispersing LPS-p in EP is caused by electrostatic repulsion; charge of LPS-p can be characterized as positive according to observation particle deposition on the cathode. Moreover, as typical behavior of EPD, decreasing current density induced by film deposition was confirmed in EP including LPS-p. Small and flat current density curve is obtained in the case of the EP with LPS-M and obvious deposition of LPS-M did not occur, indicating that LPS-M produces fewer surface charging than LPS-p; the small current density may be caused by electrophoresis of impurities.

4.3.2. Characterization of deposited film

The LPS-p film was formed on cathode by EPD under applied voltage (100 V / 0.5 cm) between ITO substrates for 20 s as shown in Fig. 4-4 (a). The film was formed homogeneously by deposition of plate like particles which can be observed in SEM image of film surface (Fig. 4-4 (b)). There is no marked agglomeration of deposited particles in the surface SEM image; On the contrary, deposited particles were well dispersed in the film morphology with micro-scale and constructed as like mesoporous structure. The same structure was distributed homogeneously in the overall cross-sectional direction of as-prepared EPD film with the thickness on order of several 10 ~ 100 μm (Fig. 4-4 (c)). The forming film with particles keeping with good dispersibility is suggesting that the well-dispersed state of LPS-p in suspension has

been retained during the processing. One of the typical features of EPD method, the film thickness can be controlled easily by varying EPD conditions such as applied time of electric field. We investigated the dependence of film thickness on applied time under applying constant current density, and its result is shown in Fig. 4-5. The film thickness was varied linearly with increasing applied time under applying constant current because of fixing the current, meaning amount of migrated particles. It was found that LPS-p film with desired film thickness can be fabricated by EPD process.

In order to determine the structure of deposited particles on the cathode, XRD measurement of the powder consisting of deposited particles (Fig. 4-6 (a')) was carried out with dispersed particles in suspension as reference (Fig. 4-6 (a)). The deposited particles had the same crystal structure with dispersed particles. Thus, dispersed particle is deposited onto cathode without any chemical changes in EPD process. We previously reported that particles of LPS precursor were converted to LPS particles with high ionic conductivity by treating at 170°C under vacuum. In addition, resulted particle shows different crystal phase after aging compared with the LPS-p. Based on the above findings, structure of deposited film (Fig. 4-6 (b')) and dispersed particles (Fig. 4-6 (b)) were compared after aging at 170°C under vacuum. The diffraction pattern of the deposited particle after treatment is attributed to thio-LISICON structure reported by Kanno et. al⁶⁾. As a consequence, LPS films were obtained by the similar process with our previous report. Obtaining LPS-p and LPS films was also confirmed from Raman spectra shown in Fig. 4-7. The observation of peak of PS_4^{3-} at 420 cm^{-1} in all specimens indicated that the chemical bond of LPS was preserved during EPD processing and aging. Typical Raman spectrum of LPS-p has peaks assigned to C-H bond attributed to ester solvent at around 2900 cm^{-1} , and these disappeared by aging because of ester evaporation from LPS-p particles. Disappearing C-H peaks was also confirmed in EPD film after aging.

4.3.3. Evaluation of conduction properties associated with Li_3PS_4 morphology

The lithium-ion conductivity of EPD film was evaluated by AC impedance measurement under various temperatures. Fig. 4-8 illustrated Arrhenius plots of EPD films and pelletized LPS powders; pelletize specimens were prepared by the conventional procedure for reference. Parameters obtained from Fig. 4-8 are indicated in Table 4-1. EPD film deposited on Al substrate after conventional aging showed lower room temperature conductivity σ_{25} ($1.8 \times 10^{-5} \text{ S cm}^{-1}$) than conventional LPS pellet ($3.4 \times 10^{-4} \text{ S cm}^{-1}$). The deposited particles have been already identified as same as pelletized LPS specimen. In other words, the lower conductivity can be ascribed to the film morphology rather than properties of deposited particles. In fact, previous SEM observation of deposited film (Fig. 4-4 (b) and (c)) presented that the film has the porous structure, which is not suitable for ion conducting generally. Thus, LPS film was treated by warm pressing at 220°C to obtain higher conductivity. EPD film with warm pressing (220°C , 30 MPa, 1 h) showed comparable conductivity ($1.9 \times 10^{-4} \text{ S cm}^{-1}$) at ambient temperature to pelletized LPS powder fabricated from LS method. Therefore EPD film with warm pressing can be utilized as lithium-ion conductor materials which have sufficiently higher conductivity. Moreover, the LPS film has a remarkably lower average of activation energy E_a (16.6 kJ mol^{-1}) compared with LPS film without warm pressing (42.5 kJ mol^{-1}) and pelletized LPS (45.5 kJ mol^{-1}). Although the similar trend is found in pelletized specimen with the warm pressing of LPS-p powder, pelletized LPS-p powder indicates a comparatively small change of E_a (31.6 kJ mol^{-1}). The effect of warm pressing of LPS-p is insufficient for the explanation of significant decreasing of E_a in LPS-film with warm pressing.

We have further examined the effect of warm pressing of LPS film by XRD and Raman spectroscopy firstly. The XRD patterns are shown in Fig. 4-9 before and after aging by vacuum heating or warm pressing of LPS-p film. A broad pattern was observed in the film aged by warm pressing, which is different from the specimen with some crystalline dried at 170°C under vacuum, indicating that amorphous like structure was formed by warm pressing. On the other hand, no change of peak attributed

to PS_4^{3-} was observed in Raman spectra, before and after each heat treatment (Fig. 4-10). According to these results, there is difference of structural regularity of PS_4^{3-} without chemical change between vacuum heating and warm pressing of LPS-p. The above observations were found equivalently in primal LPS-p powder without obvious difference. Reduced E_a in pelletized or deposited LPS-p treated with warm pressing was probably caused due to crystallographic disorder of PS_4^{3-} in the amorphous structure. Even though, large difference in E_a between EPD film and pellet has not been clarified in terms of thermostatics.

Next argument concerns kinetics of lithium ion at interfacial boundary in specimens based on electrochemical impedance spectroscopy. Fig. 4-11 is Cole-Cole plots of pelletize LPS powder with/without warm pressing. The reduced diameter of semicircle (approx. 1.7 times) and increased characteristic frequency were observed (2.26 MHz to 2.84 MHz) in spectrum of the specimen treated by warm pressing. These results indicate decreasing interfacial resistance due to grain boundary etc.; it is speculated effect of the disappearance of grain boundary in specimen is caused by amorphous structure. Fig. 4-12 (a) shows Cole-Cole plots of EPD film with/without warm pressing; (b) is magnified figure of (a) for EPD film with warm pressing. EPD film without warm pressing is inappropriate as ion conductor because of too large resistance. In contrast, as shown in Figs. 12 (a) and (b), interfacial resistance in EPD film with warm pressing treatment was remarkably decreased (approx. 80 times) and resulted resistance was equivalent to that of pelletized powder with warm pressing. Similarly, the characteristic frequency (2.84 MHz) is corresponding to the one of pelletized specimen with warm pressing, suggesting that EPD film with warm pressing was also affected by amorphous structure similarly. Additionally, the unclear semicircle compared with other spectra was recorded. It is indicating that interfacial resistance on range of higher frequency was decreased. In fact, frequency, at end of the semicircle, of EPD film with warm pressing was significantly increased (567.9 kHz) compared with other specimens (below 28.4 kHz), this character was not found in any other specimens. This result shows that reaching to diffusion-limited

access in EPD film with warm pressing is accelerated compared with other specimens; briefly, ion transport on the boundary is much easier. As a consequence, much lower E_a in EPD film with warm pressing is assumed to be associated with not only crystallographic effect but also accelerated-interfacial-ion transport as the kinetic effect.

The question we have here is why the specific kinetic effect appeared in only EPD film treated by warm pressing. It may be caused by the morphology of particles in as-deposited EPD film. Already described at the explanation of SEM images, LPS-p particles were deposited as uniform and porous film without obvious agglomeration. Because of porous structure, the as-prepared film showed poor ion conductivity owing to small contact area among particles. However, this film is being expected to the precursor of dense film. In generally, small particles such as the dispersed particle employed in current work are easily sintered. Thus, probably, improved interfacial properties were observed because of formation of dense ion conductor prepared by warm pressing EPD film. According to above explanation, forming dense materials with good contact at solid-solid interface can be achieved via EPD with suitable heat treatment.

4.4. Conclusion

This study focused on fabricating LPS film with EPD technique following with warm pressing. EPD film consisting of LPS-p was obtained successfully from as-prepared suspension of LPS-p after shaking process in LS method. Based on characterization, dispersed LPS-p was deposited on electrode without any chemical change under applied electric fields and resulted film has homogeneously distributed morphology in the overall film. LPS film obtained via warm pressing exhibited high conductivity with remarkably lower activation energy compared with conventional LPS materials. In result, the formation of good contact at the grain boundary is suggested from comparison of AC-impedance measurement.

References

- 1) H. Rahimi-Eichi, U. Ojha and F. Baronti, *IEEE Ind. Electron. Mag.*, **7**, 4-16 (2013).
- 2) F. Mizuno, A. Hayashi, K. Tadanaga and M. Tatsumisago, *Adv. Mater.*, **17**, 918-921 (2005).
- 3) Sakuda, A. Hayashi and M. Tatsumisago, *Sci. Rep.*, **3**, 2261-2265(2013)
- 4) N.H.H. Phuc, K. Morikawa, M. Totani, H. Muto and A. Matsuda, *Solid State Ionics*, **285**, 2-5 (2016).
- 5) L. Besra and M. Liu , *Prog. Mater. Sci.*, **52**, 1-61 (2007).
- 6) R. Kanno, and M. Murayama. *J. Electrochemical Society*, **148**, A742-A746 (2001).

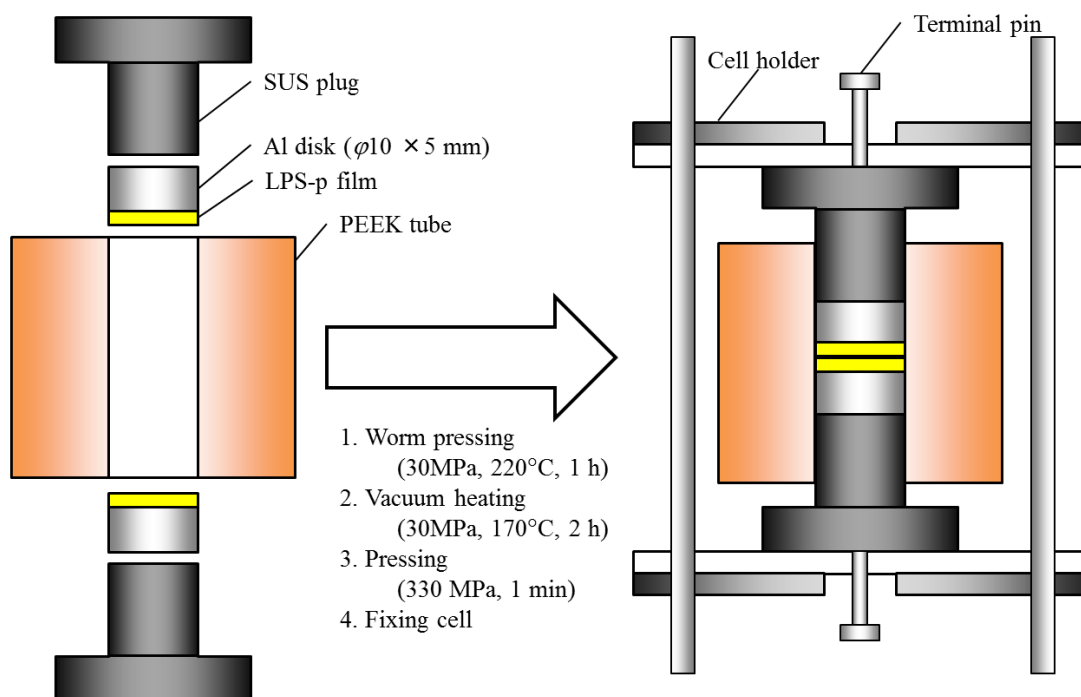


Fig. 4-1. Scheme of the cell employed for AC impedance measurement.

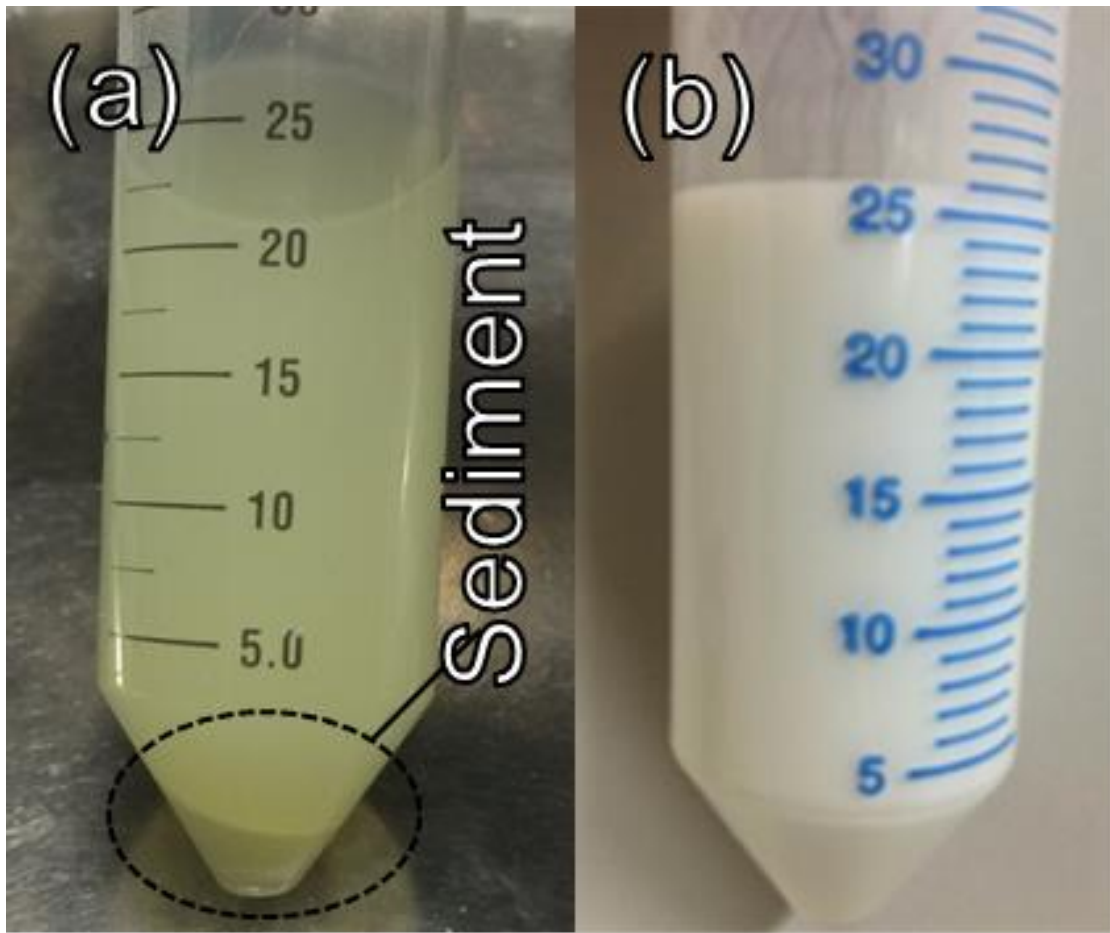


Fig. 4-2. Photographs of EP suspended with (a) LPS-M and (b) LPS-p.

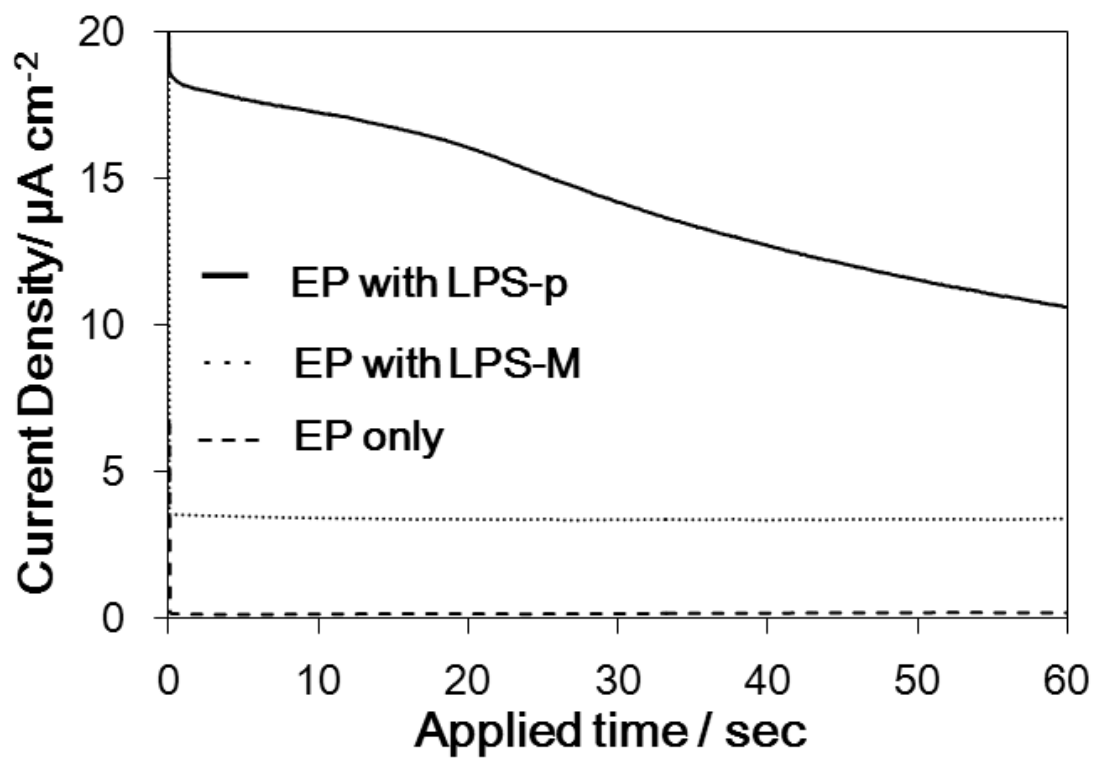


Fig. 4-3. Current curves in various suspensions under applied constant voltage of 100 V between ITO substrates separated by 0.5 cm.

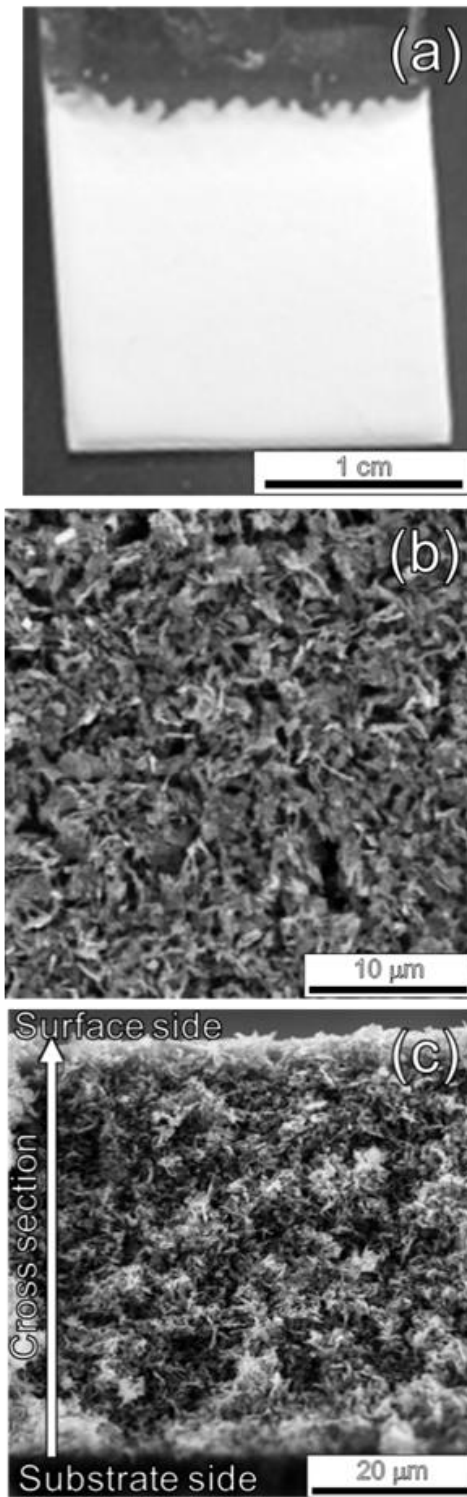


Fig. 4-4. (a) Photograph of LPS-p deposited cathode ITO substrate and its SEM images in (b) surface and (c) fracture cross-section. The film was fabricated by applied 100 V / 0.5 cm between ITO substrates for 20 s.

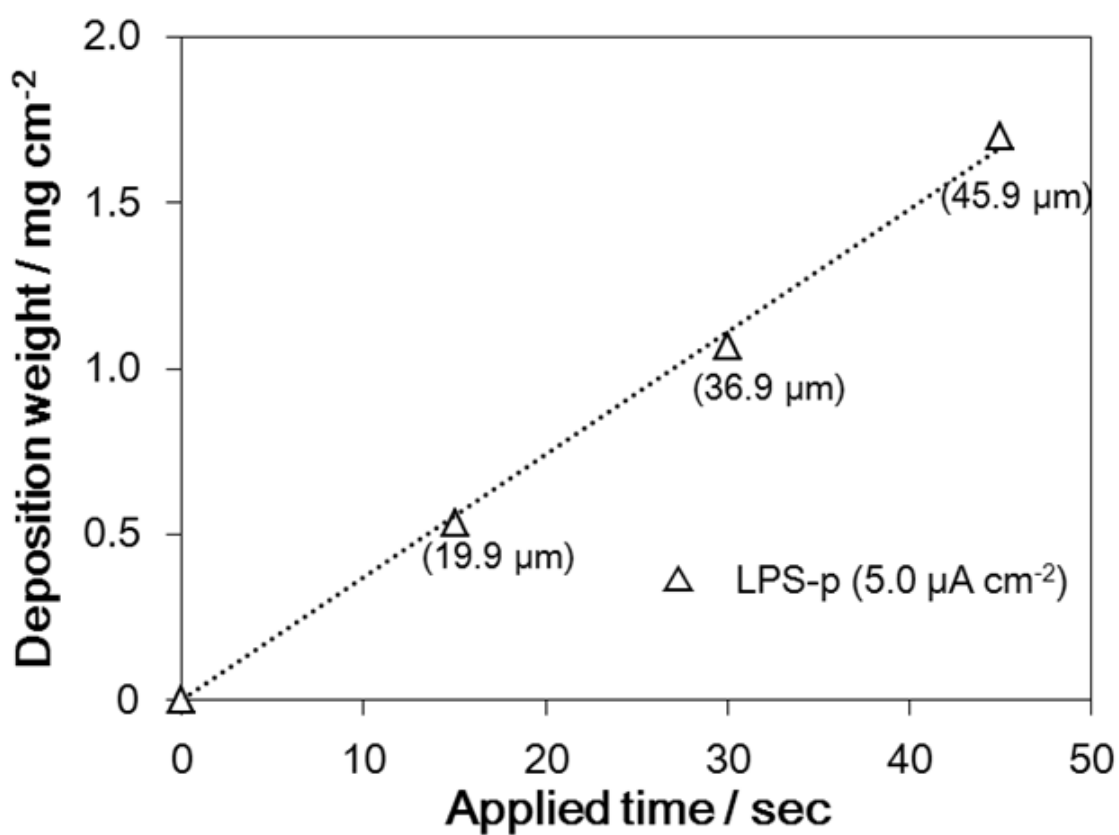


Fig. 4-5. Dependence of amount of deposition weight of LPS-p film on processing time under applied constant current density of $5.0 \mu\text{A cm}^{-2}$. Average film thicknesses are noted nearly at each plot.

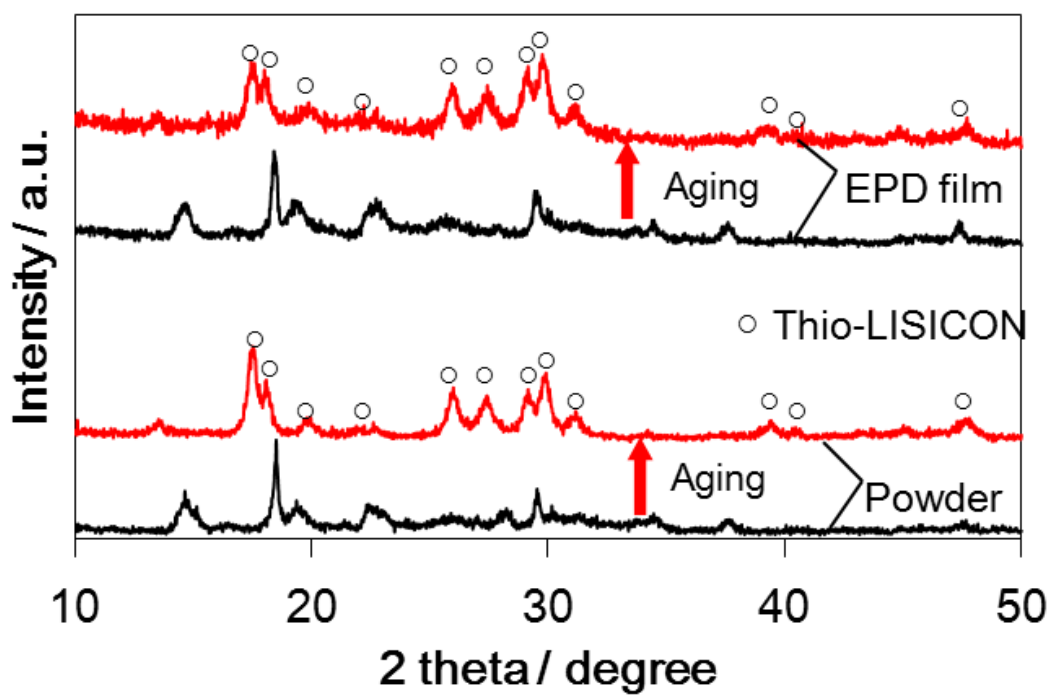


Fig. 4-6. XRD patterns of deposited particles prepared by EPD (100 V / 0.5 cm) (a') before and (b') after aging by heat treatment (170°C, about -100 kPa, for 2h). Dispersed particles recovered from suspension (a') before and (b') after aging by heat treatment are for reference.

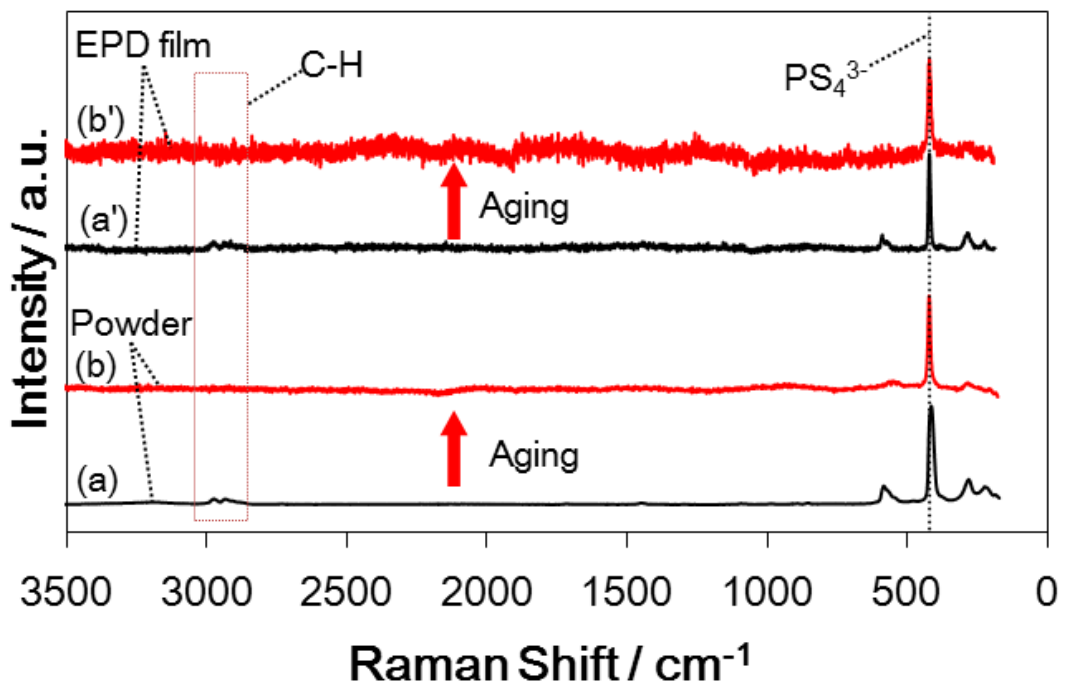


Fig. 4-7. Raman spectra of deposited particles prepared by EPD (100 V / 0.5 cm) (a') before and (b') after aging by heat treatment (170°C, about -100 kPa, for 2h). Dispersed particles recovered from suspension (a') before and (b') after aging by heat treatment are for reference.

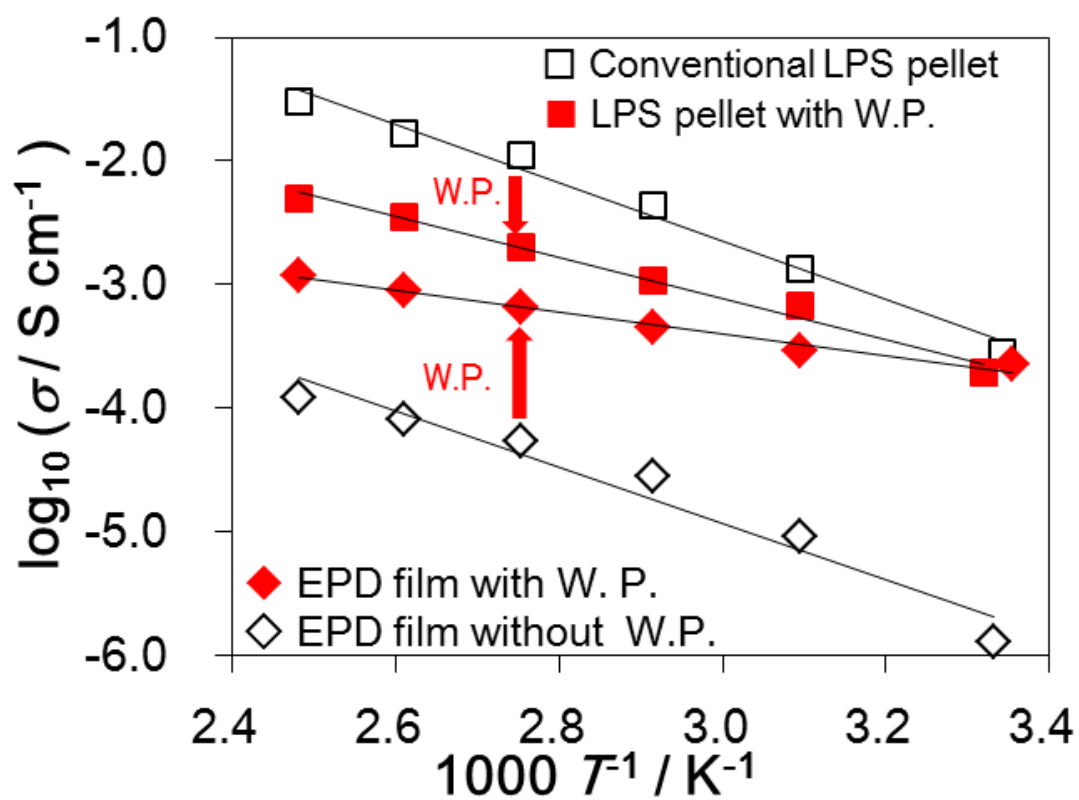


Fig. 4-8. Dependence of ion conductivity in LPS film and pelletized LPS powder with/without warm pressing (W.P.) on temperature.

Table 4-1. Parameters of ion conduction obtained from Fig. 4-8.

Sample	$\sigma_{25} / 10^4 \text{ S cm}^{-1}$	$E_a / \text{kJ mol}^{-1}$
Convent. LPS pellet	3.26	45.3
LPS pellet with W.P.	2.02	31.5
EPD film without W.P.	0.18	42.5
EPD film with W.P.	1.98	16.6

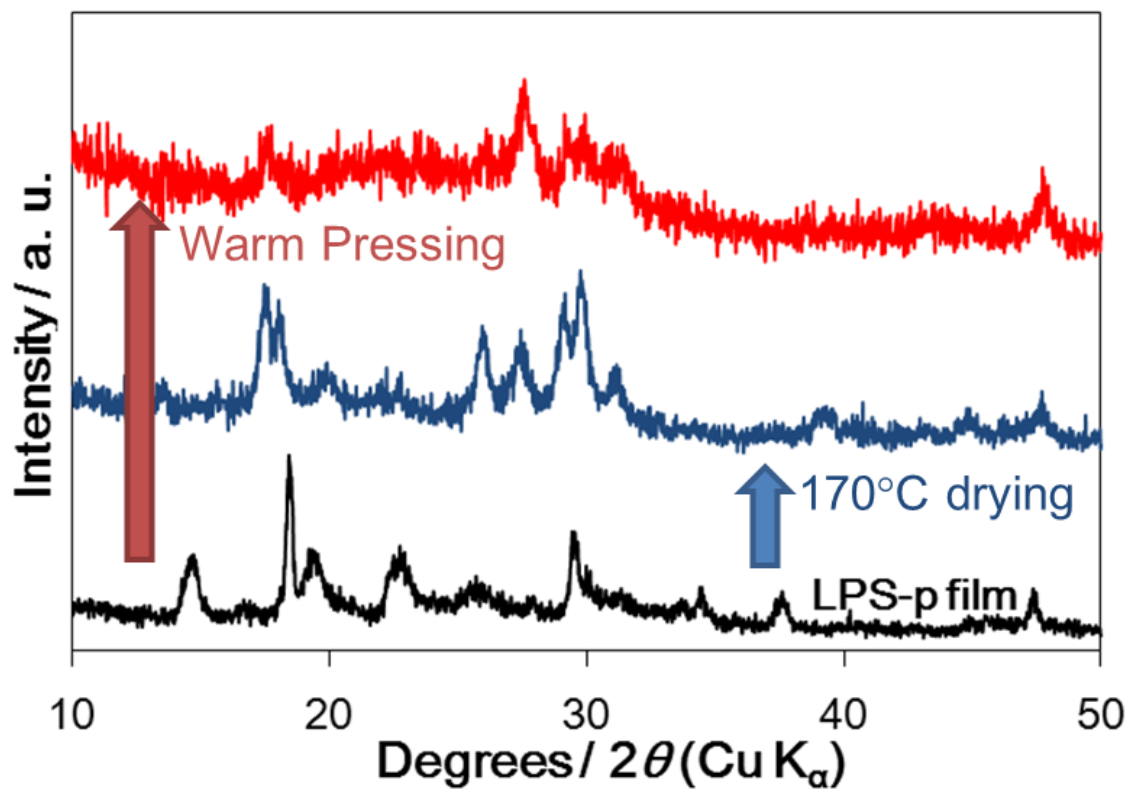


Fig. 4-9. XRD patterns of LPS-p film with/without aging by vacuum heating or warm pressing.

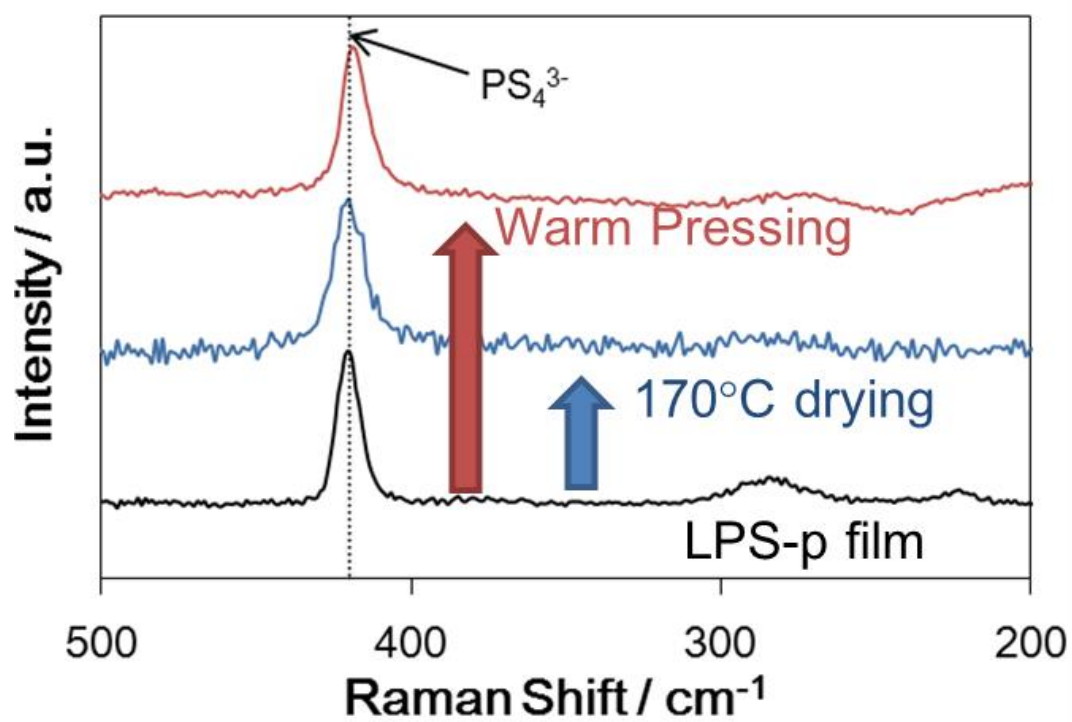


Fig. 4-10 Raman spectra of LPS-p film with/without aging by vacuum heating or warm pressing.

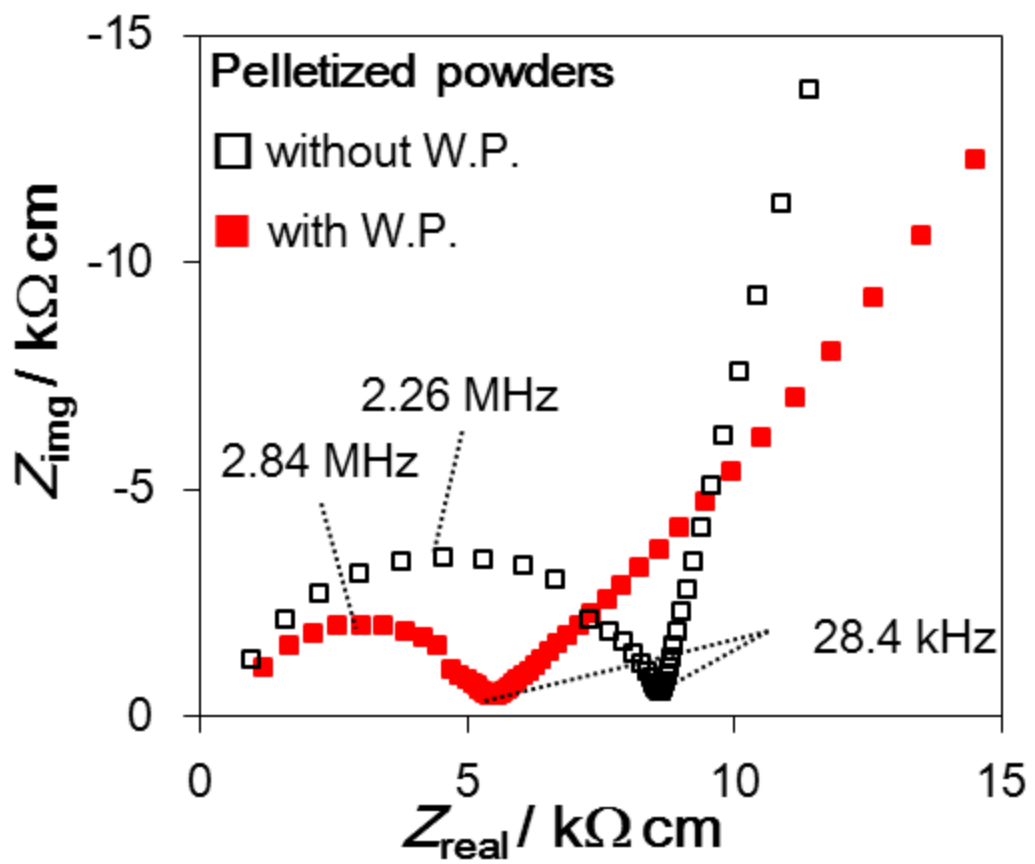


Fig. 4-11. Cole-Cole plots of pelletized LPS powder with/without aging by warm pressing under ambient temperature.

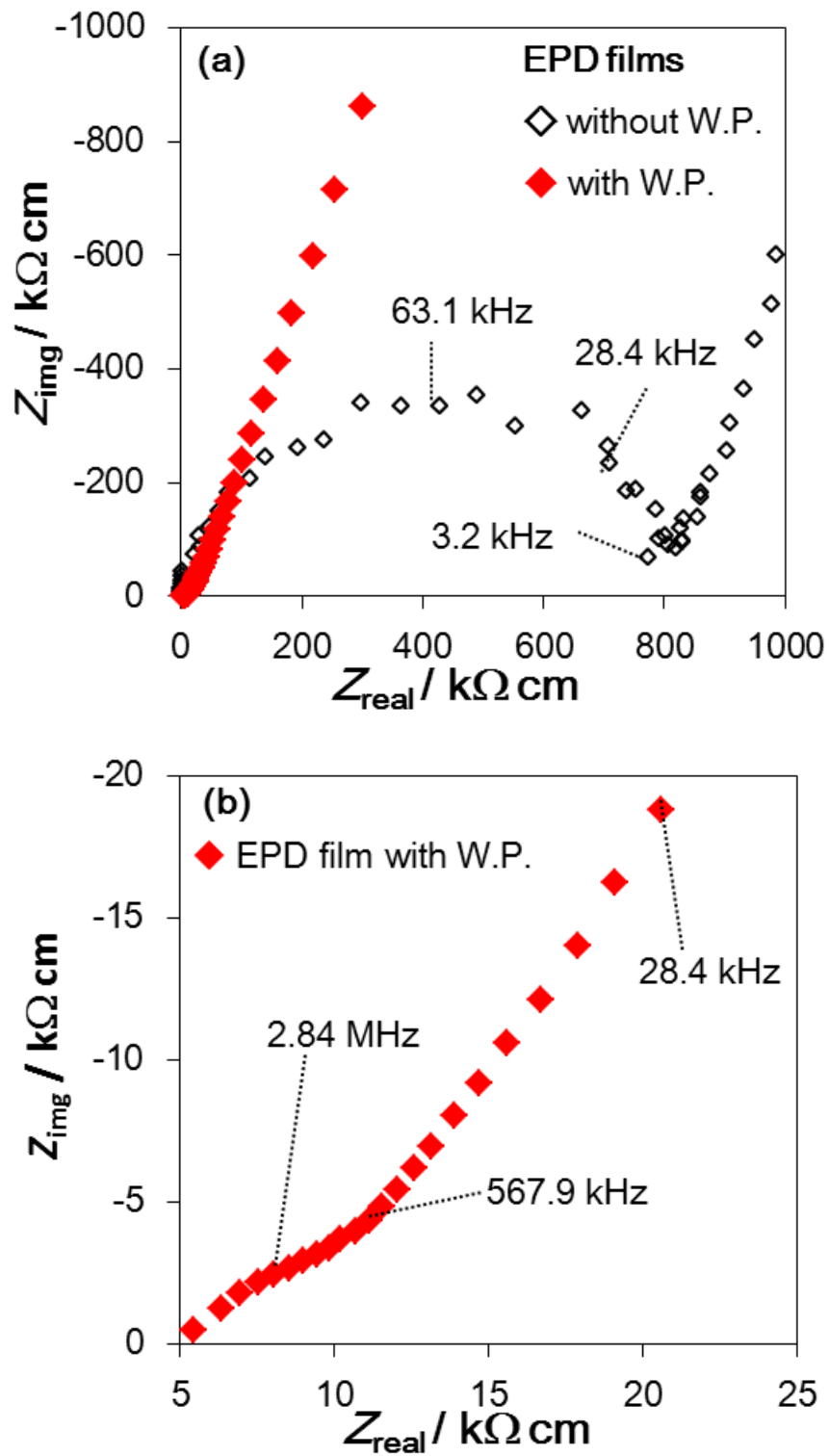


Fig. 4-12. (a) Cole-Cole plots of EPD film of LPS with/without aging by warm pressing under ambient temperature; (b) magnified plot of (a).

Chapter V

Preparation of cathodic mixture layers by alternant electrophoretic deposition process and evaluation of charge-discharge cycle performance for all solid state lithium ion batteries

5.1. Introduction

Secondary lithium ion batteries (LIBs), which have higher voltage and higher energy density than conventional batteries, are expected to be the power sources for not only mobile devices but also electrical vehicles and smart grid system^{1,2)}. In order to extend versatility, improvement of energy density and safety against ignition hazard are required for LIBs.

Recently, all-solid-state LIBs (ASS-LIBs) are proposed, which use inorganic solid-electrolyte instead of organic liquid electrolyte employed as common ion transport media in commercial LIBs. By using solid-electrolytes, due to smaller volume and stable compared with the liquid electrolytes, high energy density, downsizing of cells, expanding utilizable temperature ranges, and enhanced safety against fire breakout are resulted in LIBs. Thus, ASS-LIBs are suitable as generalized power sources in next generation. ASS-LIBs are categorized in thin film or bulk type accordance with the cell structure. In this study, bulk type ASS-LIBs are discussed. Cell capacity of this kind of LIB, of which cathode, anode, and electrolyte are constructed with various particles, can be controlled by varying amount of active-materials in electrode layer.

The key investigations for achieving bulk type AAS-LIBs with high performance are following.

- (1) Development of solid electrolytes with high lithium ion conductivity at ambient temperature.
- (2) Forming of optimized hetero-boundary between active-materials and solid electrolyte in order to suppress resistance associated with boundary charge transfer.
- (3) Well percolated ion-conducting pathway in electrode microstructure for increasing amount

of effective active-materials.

Mizuno and Sakuda reported novel sulfide lithium-ion conducting materials, as $\text{Li}_2\text{S-P}_2\text{S}_5$ (LPS), with high ambient-temperature conductivity and favorable mechanical properties for applying to ASS-LIBs^{3, 4}; LPS was employed as solid electrolyte in this study. In addition, LiNbO_3 -coated LiCoO_2 as cathode material exhibited low interfacial resistance when combined with LPS⁵), which is explained due to reduced thickness of space charge layer at hetero-boundary⁶). On the other hand, in our best knowledge, studies of electrode layer microstructure fabrication method assigned to (3) are very few despite important factor for LIB's performance; especially, it is essential problem in case of improving energy density of LIB cell by higher ratio of active materials in electrode layer. Most of studies in association with microstructure remain within mapping of each component (as like active-materials, electrolytes and conductive materials such as carbon) in just pelletize mixture powder. Conventionally, cathode mixtures with desired ratio of components in ASS-LIBs are prepared by hand mixing due to their simplicity. However, in employing this method, the components distribution in the mixture is uncontrollable; as a consequence, ratio of effective active-materials will be lower because of uniformly percolated ion conduct pathway in electrode microstructure is limited (Fig. 5-1). Thus, novel procedure which can be designing microstructure is needed for fabricating the mixture with high effective active-materials ratio.

Morphology and microstructure of obtained films by EPD can be easily controlled by controlling the processing conditions such as strength of electric field, applied time, wave shape, dispersion state, and sequence of deposition. Accordingly, if EPD technique could be applied for cathode mixture fabrication, it has possibility achieving high effective active-materials mentioned above such as shown in Fig. 5-2. Non-polar solvents without water and any polar-solvent molecular must be employed as dispersion media for active-materials and LPS to avoid LPS's side-reactions as like hydrolysis and dissolution. However, this is the tough issue in employing EPD to deposit active materials and LPS, in which stable and adjustable EPD behavior is hardly achieved in non-polar solvents due to low dielectric constant.

Therefore, procedure for EPD of active-materials and LPS has to be found as one of important challenges

In this study, various structures in deposited films were fabricated by EPD in non-polar media based suspension, and ASS-LIBs performance was tested.

5.2. Experimental

5.2.1. Preparation of dispersion of $\text{LiNi}_{1/3}\text{Mn}_{1/3}\text{CoO}_2$ and Li_3PS_4 precursor with nonpolar-solvents

$\text{LiNi}_{1/3}\text{Mn}_{1/3}\text{Co}_{1/3}\text{O}_2$ (NMC), as cathodic active material, was obtained from Toda LTD (Fig. 5-3).

Firstly, NMC surface was coated with polyquaternium D 11 (PQD11, showed in Fig. 5-4 (a)) (Aldrich) by immersing into their 5 wt.% solution. Then, The Aerosol OT[®] (AOT, showed in Fig. 5-4 (b)) was added into suspension of NMC with PQD11 for anion exchanging to prepare AOT-PQD11 coated NMC. Next, AOT-PQD11 coated NMC powder was washed with acetone for several times to remove exceeds AOT and PQD11. After drying at 110°C under vacuum (about – 100 kPa), the resultant NMC was dispersed in methylene chloride by sonication for 30 min.

The procedure of suspension of Li_2S - P_2S_5 precursor (LPS-p) was prepared according to our previous reports⁷⁾. Li_2S and P_2S_5 were purchased from Mitsuwa and Merck respectively. Ethyl propionate (EP) and 3A molecular sieves were obtained from Sigma-Aldrich. EP was dehydrated before used using 3A molecular sieves. Li_2S (0.3827 g), P_2S_5 (0.6173 g) [molar ratio $\text{Li}_2\text{S} : \text{P}_2\text{S}_5 = 3 : 1$], ethyl propionate (10 mL) and zirconia balls (diameter 4 mm, about 32 g) were mixed and shaken at an amplitude of about 1 cm at 1,500 rpm in a dry Ar atmosphere at 30°C for 6 h. The obtained suspension of LPS-p was diluted 10 times with diethyl ether and used as the deposition bath in the EPD process.

5.2.2. Fabrication of cathode mixture based on $\text{LiNi}_{1/3}\text{Mn}_{1/3}\text{CoO}_2$ and Li_3PS_4 by electrophoretic deposition

NMC and LPS-p were deposited on indium thin oxide (ITO) glass substrates (40×20×5 mm) separated by a distance 0.5 cm. Constant voltage and current were supplied by source measure unit (GS610, Yokogawa). Schemes of EPD procedure for fabricating cathode mixture is illustrated in Fig. 5-5. NMC particles are first deposited on the electrode to form a sub-monolayer. Then, followed by replacing the specimen from NMC suspension into LPS-p suspension, LPS-p particles are deposited on the so-coated films. Particularly, they would fill into the space between NMC particles. By repeating the processes above, particle-reinforced composite films were obtained employing EPD. All EPD processing was carried out by employing the automatic EPD system explained in chapter II in glove box with dry Ar atmosphere.

For the cell performance test, mixture film structured as (NMC|LPS-p)₁₀ was formed on Al disk substrate ($\phi 10 \times 5$ mm); NMC and LPS-p film are deposited by EPD under applied 100 V / 0.5 cm for 60 and 2 sec respectively. Then, obtained film was combined with pelletized LPS powder by vacuum warm pressing with 30 MPa at 220°C for 1h under -100 kPa air pressures. Finally, Indium sheet ($\phi 10 \times 0.1$ mm) was also combined with above cathode and electrolyte composites by pressing of 280 MPa.

5.2.3. Characterization of alternative stacking layer

X-ray diffraction (Ultima IV, Rigaku) with $\text{CuK}\alpha$ radiation and Raman spectroscopy (NRS-3100, Jasco) with a green laser (wavelength: 532 nm) were carried out to identify crystalline phases and local structure. The measuring film thickness and morphology observation of the deposited films was carried out using 3D laser microscope (LEXT OLS4100, OLYMPUS). The cell performance was evaluated using potentiostat (SI1287 Electrochemical interface, Solatron) in a dry Ar flow atmosphere. For the AC impedance measurement, LPS-p films deposited on Al substrate ($\phi 10 \times 5$ mm) were fabricated by EPD

with same condition to mentioned above. Heat aging of the LPS-p films was carried out via the two ways, heat treatment denoted above or warm pressing at 220°C with pressure of 30 MPa under air pressure for 2h. All film samples were uniaxial-pressed at pressure of 330 MPa. Pelletized LPS was prepared by pressing of LPS powder (80 mg) obtained from LS method at pressure of 330 MPa for reference.

5.3. Result and discussion

5.3.1. Investigation of electrophoretic deposition behavior in $\text{LiNi}_{1/3}\text{Mn}_{1/3}\text{CoO}_2$ and Li_3PS_4 precursor dispersion

Fig. 5-6 (a) shows the photograph of deposited film of NMC with PQD11-AOT binder on cathodic ITO substrate obtained in methylene chloride. The homogeneous thick film with thickness of order on several ten μm was obtained by EPD in non-polar solvent and constructed by granulated particles (Fig. 5-6 (b)), which is no obvious difference with dispersed NMC particles, as seen from SEM image (Fig. 5-3). The deposited NMC particles have same crystal structure with pristine NMC dispersed in MC as shown XRD in Fig. 5-7, meaning that any chemical degradation is not observed during EPD process. Fig. 5-8 indicates correlation between film thickness and EPD time. The thickness of deposited films is adjustable linearly by varying EPD time; indicating that this deposition was behavior as typical EPD. Generally, in non-polar solvents as dispersion media, obtaining thick film is difficult because of none generated surface charge on particle surface. Here we found the procedure for EPD of thick film with controllable thickness in non-polar media by using novel binder type surfactant with ionizing and lipophilicity. LPS-p films were successfully prepared by EPD via liquid shaking method as described in chapter III.

5.3.2. Deposition of alternatively stacked $\text{LiNi}_{1/3}\text{Mn}_{1/3}\text{CoO}_2$ and Li_3PS_4 layer

Fig. 5-9 shows the cross sectional images of deposited films on ITO substrate with laminate structure based on LPS precursor(LPS-p, white layer) and NMC (black layer) fabricated by alternative EPD in each

suspension. As illustrated in Fig. 5-9, laminate structure of NMC and LPS-p was clearly observed. Additionally, number of each layer can be changed by adjusting EPD conditions as presented in Fig. 5-9 (b). For applying this film as cathode in ASS-LIBs, multilayered structure with controlled sub-monolayer should be achieved for forming contact among each of the component particles. Correlation of EPD films weight to number of deposited layers is shown in Fig. 5-10; the total film thickness and amount of deposition were varied on depending processing time. In according to above results, design of specific microstructure, such as the thickness of each layer and their total number in the film with NMC and LPS-p were possible by adjusting detail conditions. Based on these results, optimized microstructure of the films was obtained by turning EPD conditions (Fig. 5-11). NMC particles were well dispersed in LPS-p matrix like particle-reinforced materials as shown in surface image. Each layer was formed as sub-monolayer in the resulting film; average volume ratio of NMC and LPS-p was calculated as approximately 55% and 45% respectively from those images by image analysis. Moreover, NMC ratio was probably increased by warm press treatment due to volume reduction of LPS-p upon densification; actually, reducing volume of LPS-p film by the treatment was confirmed in previous study (thicknesses before and after treatment were 400 μm and 70 μm , respectively). Thus, cathode film with high ratio of NMC could be obtained by present procedure via EPD and warm pressing.

5.3.3. Charge-discharge cycle performance of cathodic mixture layer fabricated alternative electrophoretic deposition process

Fig. 5-12 shows result of cell performance test using the obtained cathode film shown Fig. 5-11 treated with warm pressing. The charge / discharge coulombic efficiency of 58% were observed in the as-prepared ASS-LIB cell. Therefore, the NMC-LPS film fabricated via EPD can be applied as cathode in ASS-LIBs. In order to enhance the cell performance, optimization of microstructure of the film is necessary; for instance ratio of NMC and LPS, their distribution etc.

5.4. Conclusion

In this study, films of NMC and LPS-p with controllable thickness were successfully prepared by EPD for the first time. Furthermore, films with NMC and LPS-p alternative layers were also obtained by alternant EPD process. The microstructure of prepared film was controllable by EPD conditions. The film obtained via EPD followed by warm pressing was tested as cathode of ASS-LIBs, and the results proved that proposed EPD procedure can be employed for electrochemical devices fabrication, i.e. ASS-LIBs.

References

- 1) J.W. Fergus, *J. Power Sources*, **195**, 4554-4569 (2010).
- 2) H. Rahimi-Eichi, U. Ojha, F. Baronti, *IEEE Industrial Electronics Magazine*, **7**, 4-16 (2013).
- 3) F. Mizuno, A. Hayashi, K. Tadanaga, M. Tatsumisago, *Advanced Materials*, **17**, 918-921 (2005).
- 4) A. Sakuda, A. Hayashi, M. Tatsumisago, *Scientific Reports*, **3**, 2261-2265 (2013)
- 5) N. Ohta, K. Takada, I. Sakaguchi, L. Zhang, R. Ma, K. Fukuda, M. Osada, T. Sasaki, *Electrochem. Commun.*, **9**, 1486-1490 (2007).
- 6) J. Haruyama, K. Sodeyama, L. Han, K. Takada, Y. Tateyama, *Chemistry of Materials*, **26**, 4248-4255 (2014).
- 7) N.H.H. Phuc, K. Morikawa, M. Totani, H. Muto, A. Matsuda, *Solid State Ionics*, **285**, 2-5 (2016).

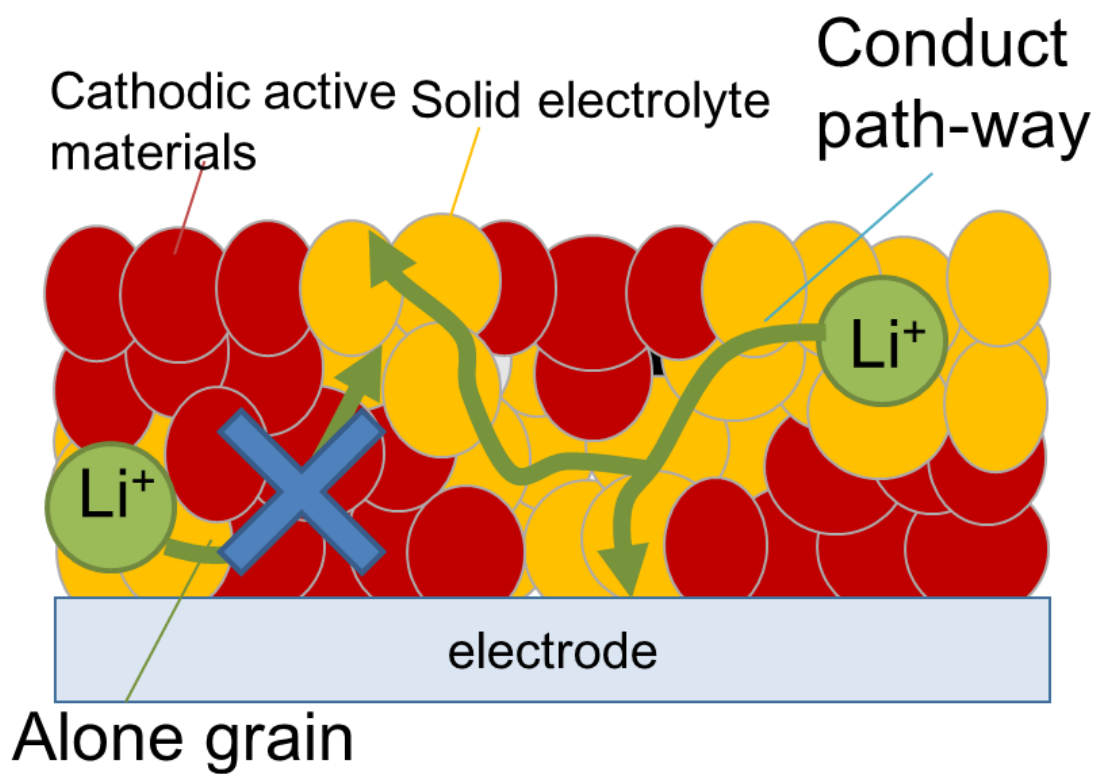


Fig. 5-1. Scheme of microstructure in cathode mixture based on cathodic active materials and solid electrolyte, fabricated by conventional mechanical mixing, and effective or not solid electrolyte grain for lithium ion conduction.

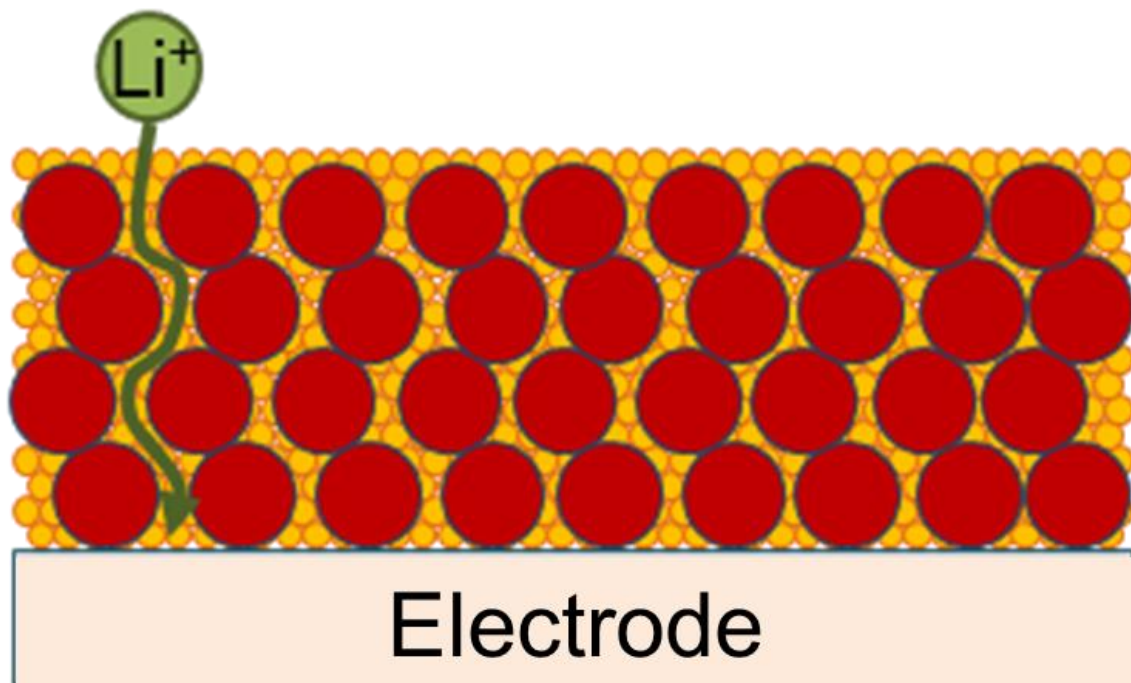


Fig. 5-2. Scheme of target microstructure in cathode mixture based on cathodic active materials and solid electrolyte, fabricated by EPD suggested in this work and effective lithium ion conduction path.

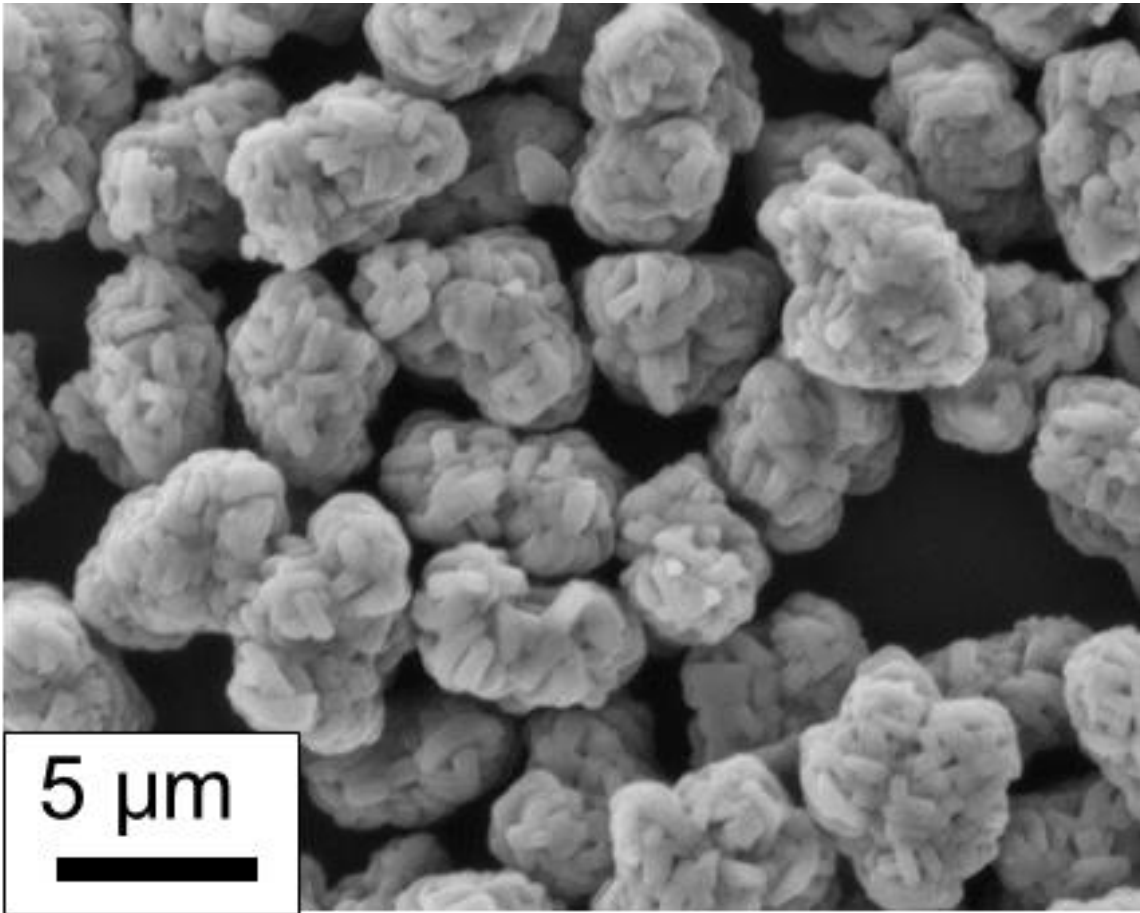


Fig. 5-3. SEM image of as-received NMC particles.

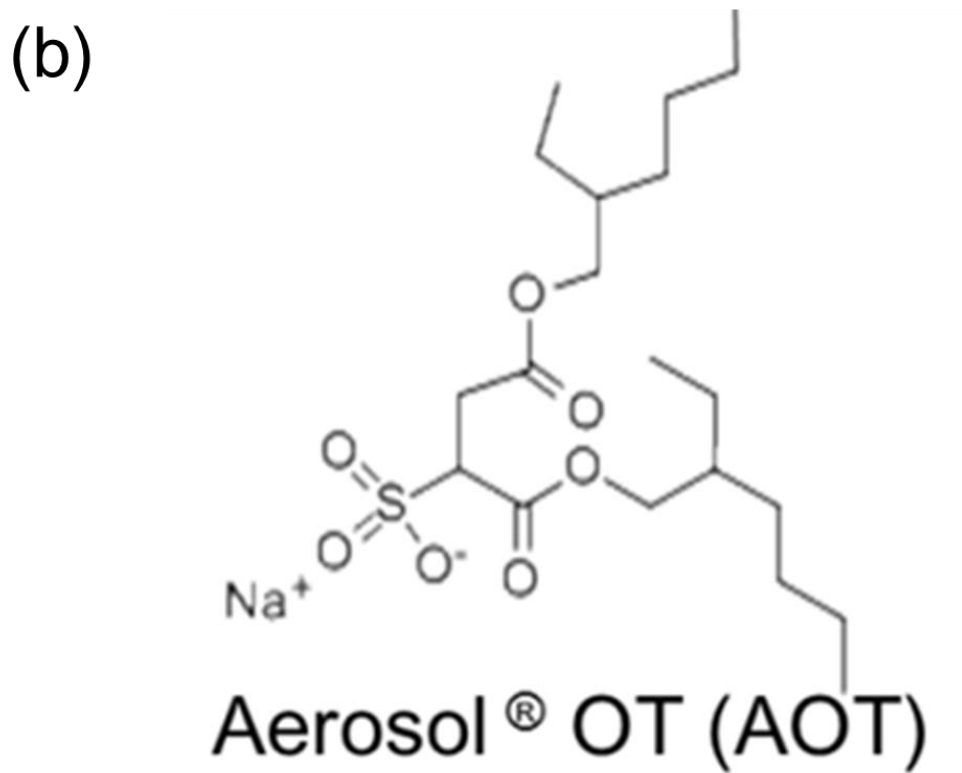
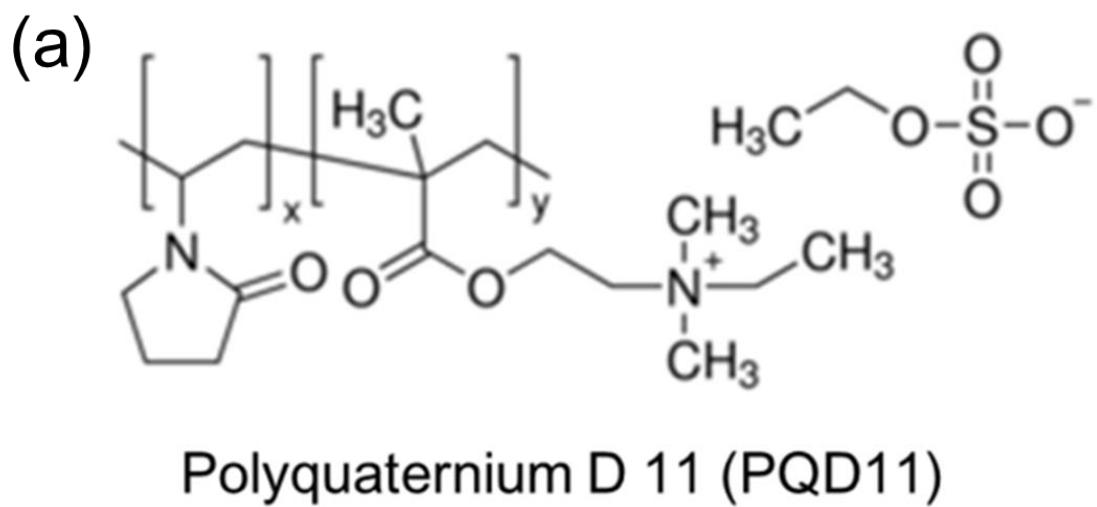


Fig. 5-4. Chemical structure of (a) Polyquaternium D11 (PQD11) and (b) Aerosol[®] OT (AOT).

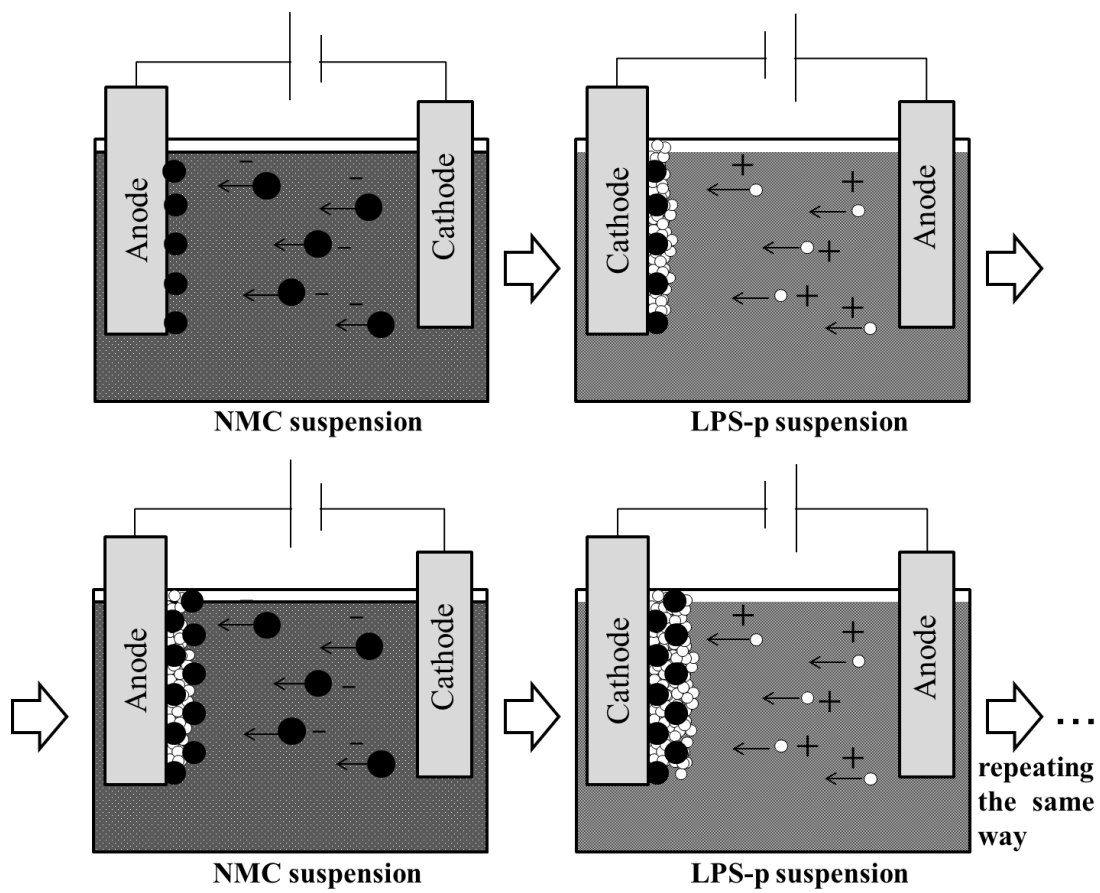


Fig. 5-5. Scheme of fabrication procedure for particle-reinforced composite films using EPD.

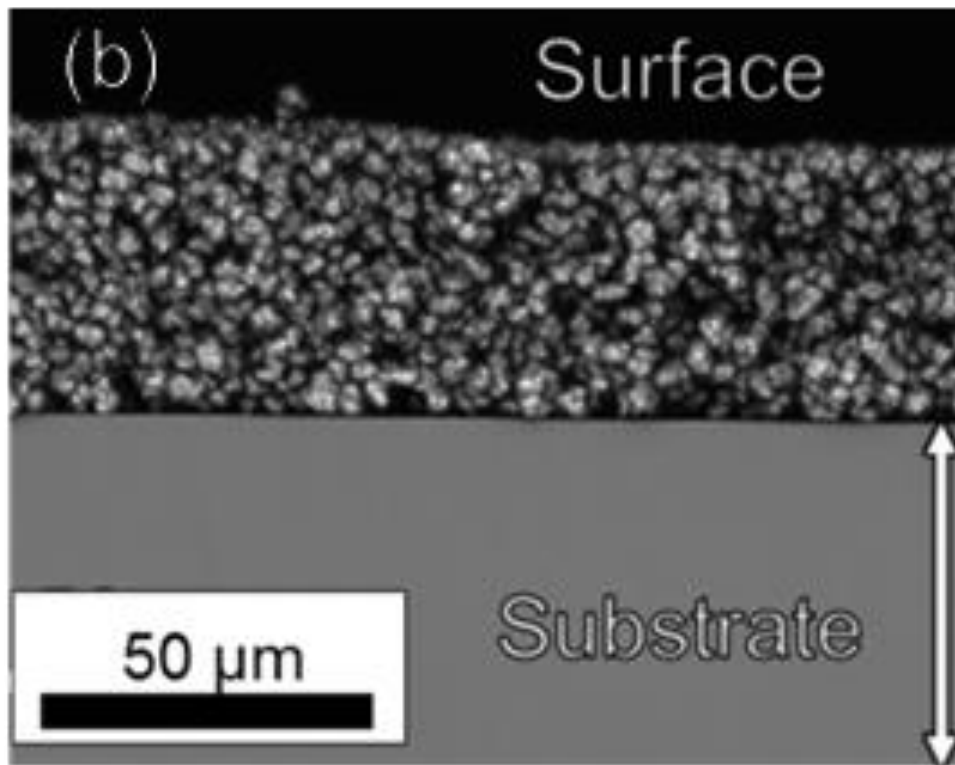
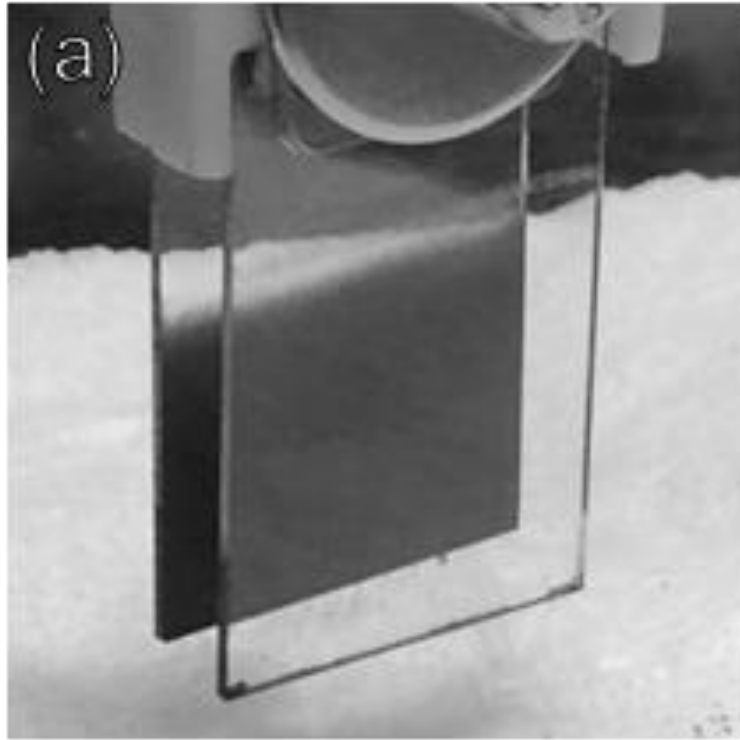


Fig. 5-6. Photograph of (a) anodic deposition of NMC on ITO and (b) SEM image on cross-section of deposited NMC film.

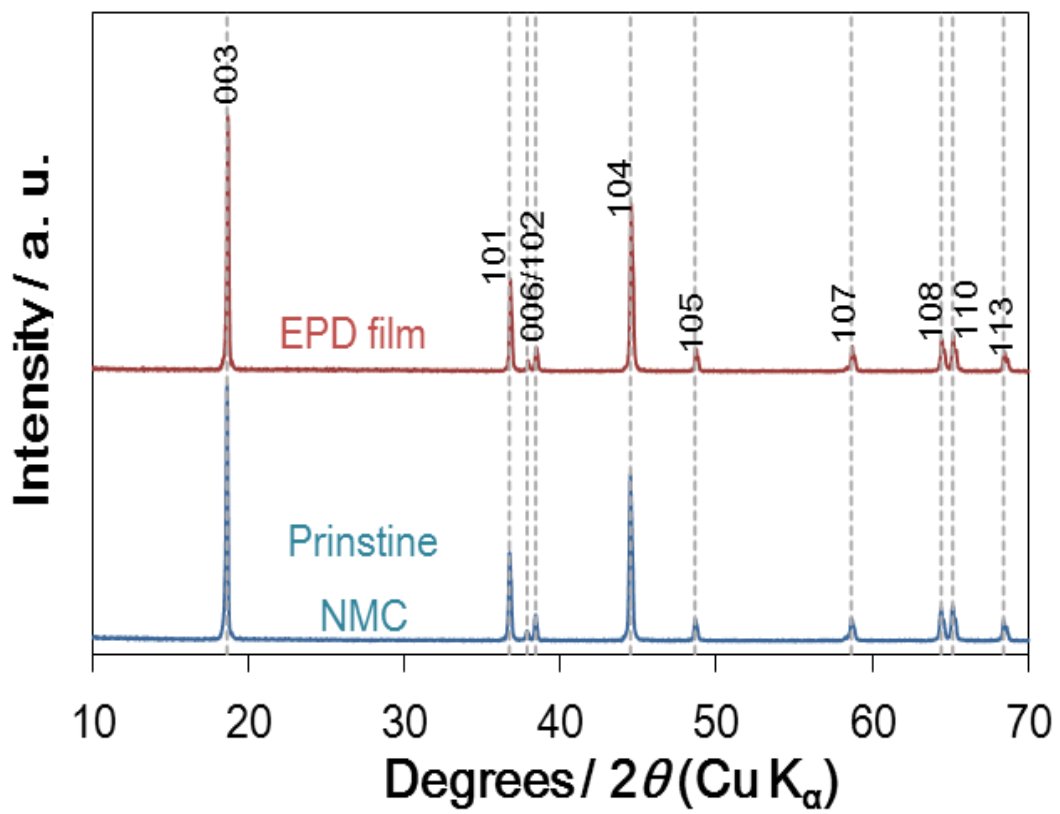


Fig. 5-7. XRD pattern of EPD film based on NMC particles; the pattern of pristine NMC is for reference.

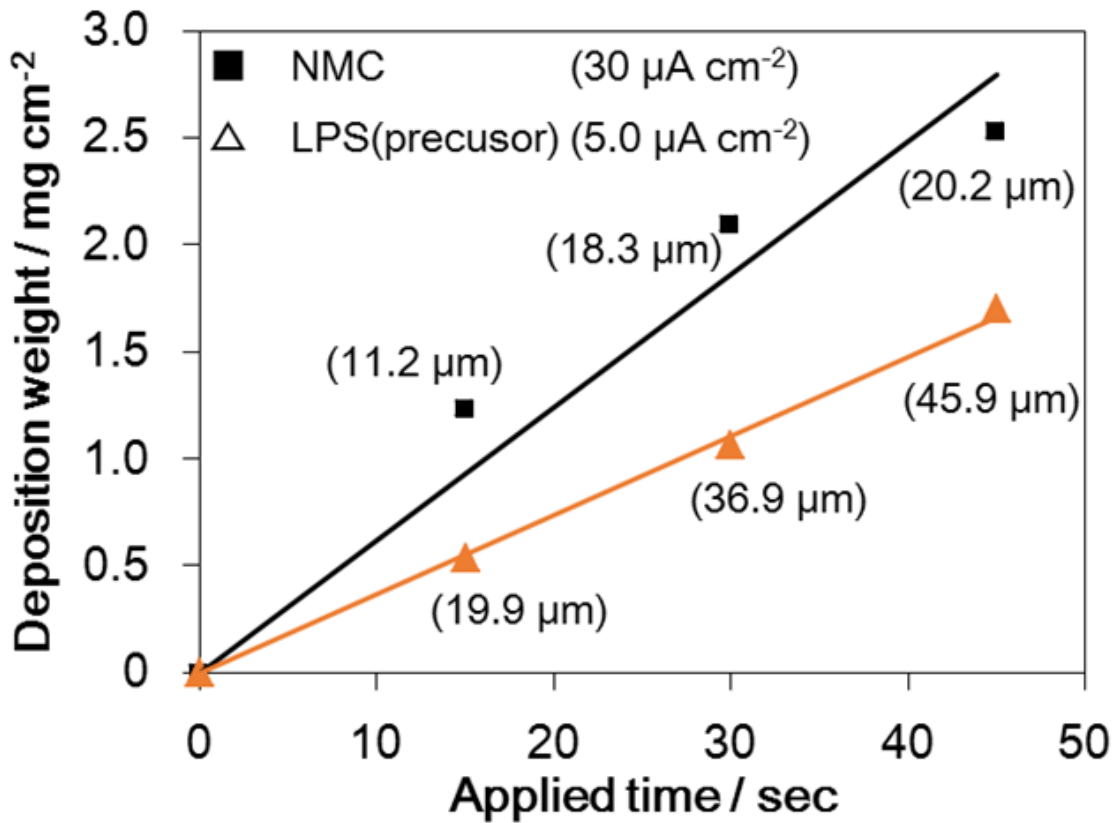


Fig. 5-8. Correlation of EPD films weight to number of deposited layers under constant voltage for NMC. Average thickness of deposited films on each plot is indicated near the plotted linear line. The plots of LPS precursor, same with Fig. 5-4 illustrated in Chapter III, is for reference.

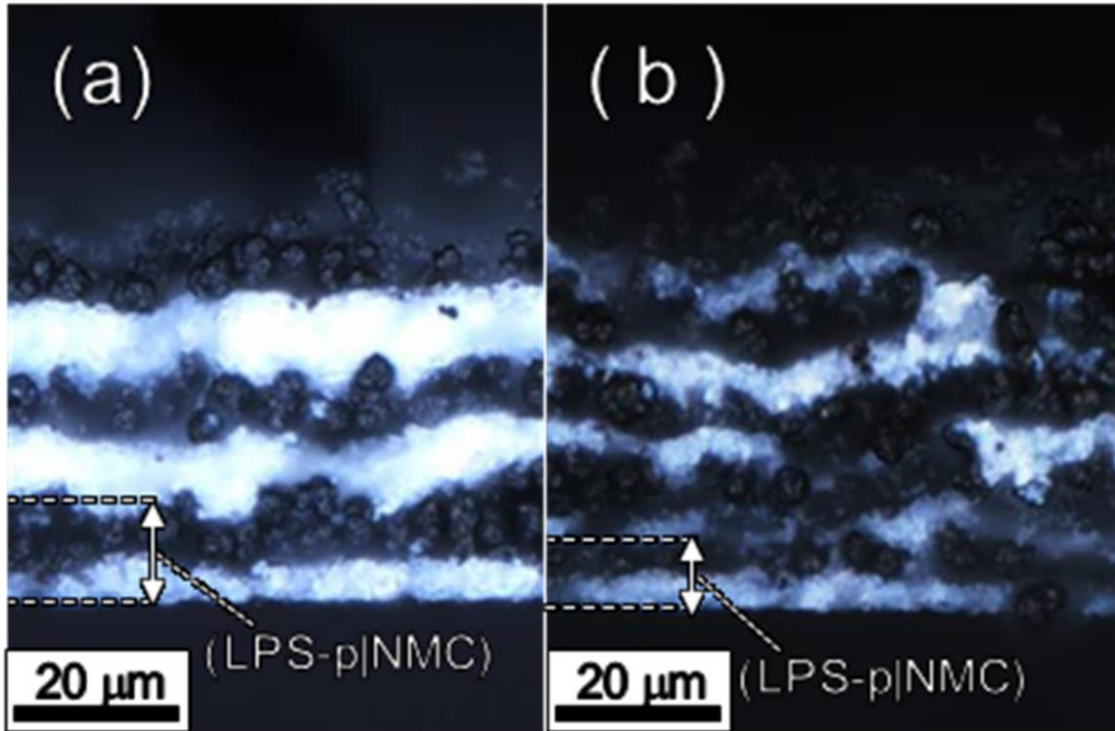


Fig. 5-9. Cross-sectional images of deposited films on ITO substrate with laminate structure based on LPS precursor(LPS-p, white layer) and NMC (black layer) fabricated by alternative EPD in each suspension; (a) three layers of (LPS-p|NMC) using deposition time of 45 sec for each layer and (b) five layers of (LPS-p|NMC) using deposition time of 15 sec for each layer.

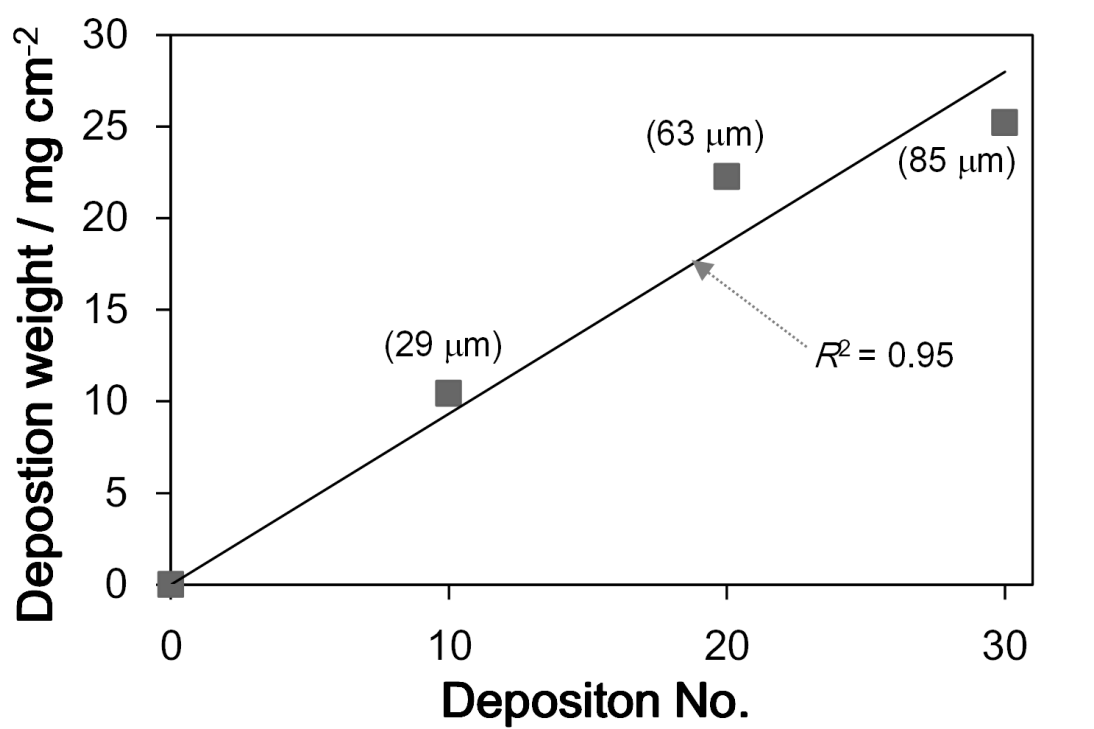


Fig. 5-10. Correlation of EPD films weight to number of deposited layers under constant voltage for NMC and LPS precursor. Average thickness of deposited films on each plot is indicated near the plotted linear line.

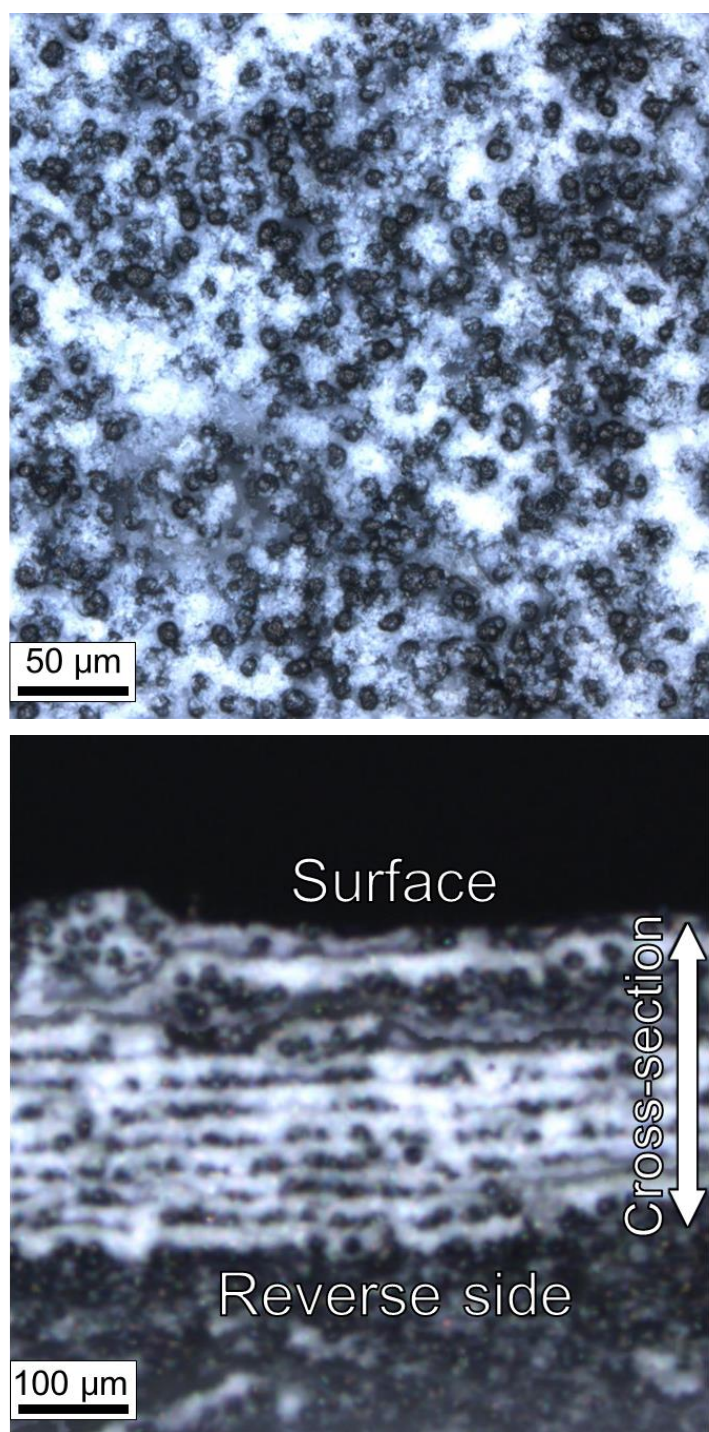


Fig. 5-11. The (a) surface and (b) cross-sectional images of deposited films on Al disk substrate with laminate structure as $(\text{NMC}|\text{LPS-p})_{10}$ based on LPS precursor(LPS-p, white layer) and NMC (black layer) fabricated by alternant EPD in each suspension; NMC and LPS-p particles were deposited under applied 100 V / 0.5 cm for 60 and 2 sec respectively.

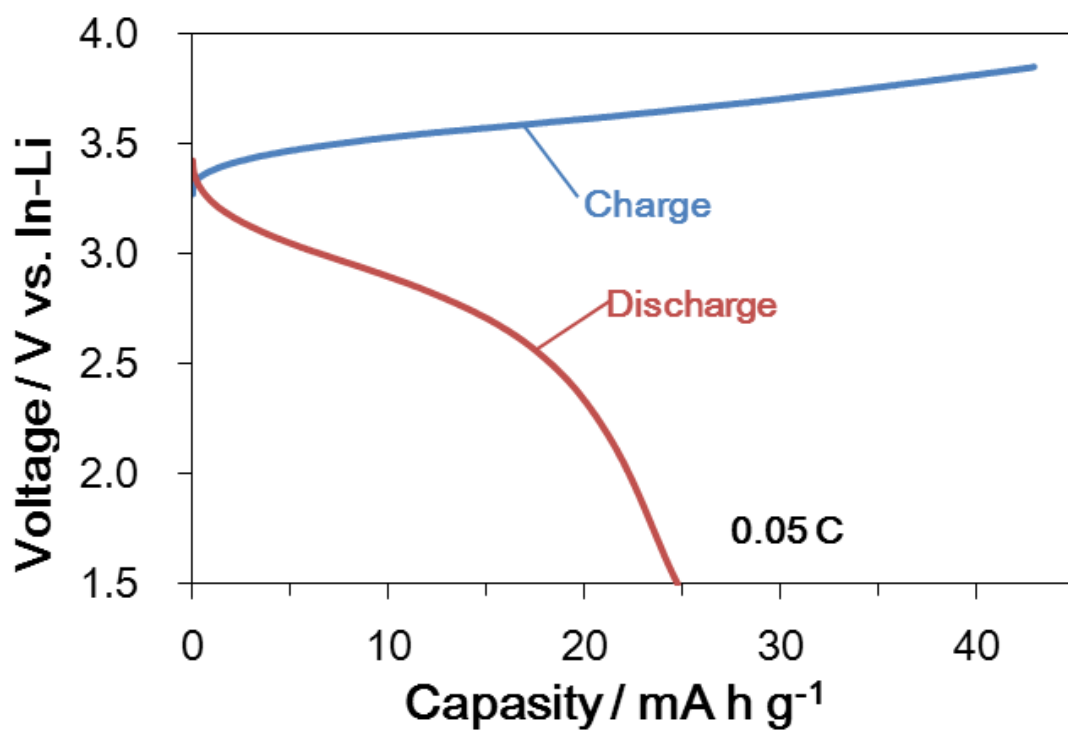


Fig. 5-12. Charge / discharge curves of ALL-LIBs with cathode fabricated via EPD.

Chapter VI

General Conclusion

In this work, applications of EPD in the preparation of electrochemical devices, mainly photoelectrochemical cells and all-solid-state lithium ion batteries, are explored. In result, base of preparation processes based on EPD for functional materials with various nano/micro structures were developed. Various materials structures in nano/micro scale were extensively designed by using EPD technique with optimized conditions for each structure fabrication. According to our results obtained, electrochemical devices fabricated by the EPD technique show a potential of practical applicability of these devices with more improvement in the EPD procedure used.

1. The automatic EPD system including coating, drying and washing processes, effective fabrication of multilayered films, which are one of the target structures in the EPD, was demonstrated. As a result, smooth multilayered films without any defects were prepared by using this system. The specific microstructures such as the thickness of each layer and their number in total were controllable by adjusting detail conditions. The performance of the system has been proved to be qualified for multilayered films preparation. Moreover, we proposed utilizing this system to fabricate particle-reinforced composite films.

2. As study case of performance evaluation of functional film with controlled nanostructure NiTi-LDH/rGO films with thickness of approximately 2–14 μm were prepared on FTO by the EPD method. In addition, the films obtained were dense with certain level of orientation due to the introduction of rGO. The NiTi-LDH/rGO|FTO showed a higher photovoltage compared to that of pristine NiTi-LDH|FTO. The highest V_{ph} was obtained in the film containing 1.0 wt.% rGO. Kinetic parameters

were obtained by fitting analysis of the transient photovoltage and Cole–Cole plots. From our analysis, it was found that conflicting effects where two opposing reaction rates for V_{ph} are introduced by compositing with rGO. Consequently, the V_{ph} of the electrode prepared with a NiTi-LDH/rGO composite film is improved. The expected effects due to the nanocomposite structure were also observed substantially in the performance of the composites-based EPD films employed as photoanode, which showed highly sensitive in both their structure nanoscale structure and microscale structure.

3. In order to prepare film based on polar-materials such as sulfide solid electrolyte by EPD in non-polar media, the EPD film consisting of LPS-p was obtained successfully from as-prepared suspension of LPS-p after shaking process in LS method. Based on characterization, dispersed LPS-p was deposited on electrode without any chemical change under applied electric fields, and resulted film has homogeneously distributed morphology in the overall film. LPS film obtained via warm pressing exhibited high conductivity with remarkably lower activation energy compared with conventional LPS materials. In result, the formation of good contact at the grain boundary is suggested from comparison of AC-impedance measurement.

4. Films of NMC and LPS-p with controllable thickness were successfully prepared by EPD for the first time. Furthermore, films with NMC and LPS-p alternative layers were also obtained by alternant EPD process. The microstructure of prepared film was controllable by EPD conditions. The film obtained via EPD and warm pressing was tested as cathode of ASS-LIBs, and the results proved that proposed EPD procedure can be employed for electrochemical devices fabrication, i.e. ASS-LIBs.

It can be concluded that EPD fabrication of functional materials for electrochemical devices is promising due to controllable nano/microstructure and their production in macro scale.

Acknowledgements

I would like to appreciate my supervisor, Prof. Dr. Atsunori Matsuda, for his constant supports and teaching during my study at the master course to doctoral course in Toyohashi University of Technology (TUT). I also would like to thank Prof. Dr. Hiroyuki Muto (TUT), Prof. Dr. Noriyoshi Kakuta in Wakayama National College of Technology, Assist. Prof. Dr. Go Kawamura (TUT), Assoc. Prof. Dr. Takanori Mizushima (TUT), Dr. Tetsuo Uchikoshi (National Institution for Materials Science) and Dr. Hideto Yamada (TUT) deeply for their helpful advice, comments, and suggestions.

I want to express gratitude to all students, graduates and researchers in Matsuda-Muto-Kawamura Laboratory at Toyohashi University of Technology.

Financial support for part of work was provided by the Advanced Low Carbon Technology Research and Development Program, Specially Promoted Research for Innovative Next Generation Batteries (ALCA-SPRING) from Japan Science and Technology Agency (JST).

We acknowledged Shinko Denso Co. Ltd. to help the developing the EPD system.

Finally, I deeply appreciate my family for their sincere encouragement. Special thanks for giving me the chance to study in the Ph.D. course.

2017, February, Shota Azuma

List of publications

[1] S. Azuma, G. Kawamura, H. Muto, N. Kakuta and A. Matsuda, "Preparation of layered double hydroxide and its graphene composite films as electrodes for photoelectrochemical cells", *Key Engineering Materials*, **616**, pp. 129-133 (2014).

[2] S. Azuma, K. Aiyama, G. Kawamura, H. Muto, T. Mizushima, T. Uchikoshi and A. Matsuda, "Colloidal processing of $\text{Li}_2\text{S-P}_2\text{S}_5$ films fabricated via electrophoretic deposition methods and their characterization as a solid electrolyte for all solid state lithium ion batteries", *Journal of the Ceramic Society of Japan*, 2016 (Accepted, 2017.1.16)

[3] S. Azuma, H. Yamada, G. Kawamura, H. Muto, T. Mizushima, T. Uchikoshi and A. Matsuda, "Development of multilayer coating system based on electrophoretic deposition process", *Journal of the Ceramic Society of Japan*, (Accepted, 2017.1.29).